IPP-Report

Max-Planck-Institut für Plasmaphysik

Johannes Illerhaus

Estimation, Validation and Uncertainty of the Position of the Separatrix Contour at ASDEX Upgrade

IPP 2019-08
April 2019


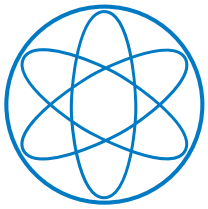


Diploma Thesis at the
Technische Universität München

Estimation, Validation and Uncertainty of the Position of the Separatrix Contour at ASDEX Upgrade

by

Johannes Illerhaus

October 23, 2018

First referee: Prof. Dr. U. Stroth

Second referee: Prof. Dr. R. Neu

Supervisor: Dr. R. Fischer

Abstract

To properly describe magnetic equilibria in fusion research it is important to be able to accurately reconstruct the position of the last closed flux surface, the separatrix. Data from sources such as the scrape-off layer (SOL) currents onto the divertor plates and the prescribed currents in the poloidal field coils are used to apply constraints to this reconstruction. But for a lot of these quantities the uncertainty is not precisely known or its influence on the separatrix reconstruction not completely understood. For this reason, a systematic investigation is necessary. In this thesis the goal is to understand the uncertainty and sensitivity of the reconstructed separatrix position to various input quantities and their uncertainties, e.g., the uncertainties in the magnetic data or the prescribed coil currents. Different magnetic probe arrays will be used as a source of the measured poloidal magnetic field to better understand the influence the uncertainty in their measured magnetic field has on the equilibrium reconstruction. A closer look will also be taken at the fast-ion modeling and its influence on the reconstructed separatrix. Finally the influence of the modeling of scrape-off layer currents on the reconstructed separatrix will be analyzed. The result will be an uncertainty quantification of the separatrix contour. The separatrix position will be validated using the Thomson scattering (TS) diagnostic and a two-point model estimation of the separatrix temperature at the midplane and the thermography diagnostic at the lower and upper divertor. These diagnostics will be used in conjunction with each other to obtain complementary information to more accurately validate the separatrix over larger parts of its contour. The study of these uncertainties should help quantify the different uncertainties and thus improve the reliability of the separatrix reconstruction.

Abstrakt

Um magnetische Gleichgewichte in der Fusionsforschung richtig beschreiben zu können ist es wichtig die Position der letzten geschlossenen Flussfläche, der Separatrix, genau rekonstruieren zu können. Daten von Messungen wie den Randschichtströmen auf die Divertorziegel, sowie die Vorschriften für Ströme in Poloidalfeldspulen werden dazu benutzt um Zwangsbedingungen für die Gleichgewichtsrekonstruktion anzuwenden. Aber für viele dieser Größen ist die Ungenauigkeit, sowie ihr Einfluss auf die Separatrixrekonstruktion nicht vollkommen verstanden. Aus diesem Grund ist eine systematische Untersuchung dieser Effekte notwendig. In dieser Arbeit ist das Ziel die Unsicherheit, sowie die Empfindlichkeit der Position der rekonstruierten Separatrix auf unterschiedliche Eingangsparameter, wie zum Beispiel die Unsicherheit in den Magnetfelddaten und die Vorschriften für die Spulenströme, zu quantifizieren. Unterschiedliche Spulenkränze werden als Quelle der magnetischen Poloidalfeldmessung genutzt werden um den Einfluss des gemessenen Magnetfeldes auf die Separatrixrekonstruktion besser verstehen zu können. Die Modellierung des Drucks der schnellen Teilchen wird auch näher betrachtet werden und ihr Einfluss auf die rekonstruierte Separatrix untersucht werden. Letztlich wird noch der Einfluss der Modellierung der Randschichtströme auf die Separatrixposition untersucht werden. Das Ergebnis dieser Untersuchungen wird eine Empfindlichkeitsquantifizierung der Separatrixkontur sein. Die Separatrixposition wird mittels der Thomsonstreuungsdiagnostik sowie einer Abschätzung der Separatrixtemperatur basierend auf dem Zweipunktmodell an der Mittelebene der Niederfeldseite validiert werden. Am oberen und unteren Divertor wird eine Validierung durch die Thermographiediagnostik durchgeführt werden. Diese Diagnostiken werden in Kombination miteinander benutzt werden um ergänzende Informationen zu erhalten. Diese Kombination wird dann eine Validierung der Separatrix auf unterschiedlichen Teilen ihrer Kontur ermöglichen. Die Untersuchung dieser Unsicherheiten sollte dabei helfen die unterschiedlichen Unsicherheiten zu quantifizieren und die Verlässlichkeit der Separatrixrekonstruktion zu verbessern.

Contents

Chapter 1

Introduction

The unsustainable rise of energy consumption and the increasing presence of climate change are two of the most pressing problems in the 21^{st} century. Fusion energy is one of the most promising candidates for solving both of these by providing a sustainable, safe and clean energy source. Fusion power plants could provide a constant backbone to the already established power grid without the need for a complete overhaul and the addition of enormous energy storage facilities that would be needed if the electrical grid was to be based on renewable energy only.

For fusion research to be able to progress at a fast pace, researchers need access to easily interpretable data and powerful tools for data analysis. But the most accurate measurements and diagnostics are useless if the scientists analyzing the data do not have a clear picture of how their measurements are positioned in the plasma and how the plasma they are analyzing behaves during a discharge.

For this reason reliable reconstruction of the magnetic equilibrium of the plasma is an integral part of fusion research. Equilibrium reconstruction uses data measured during discharges and estimates the evolution of the plasma. Data is taken from many sources such as measurements of diagnostics and modeling results in an effort to provide the most accurate equilibrium possible. But many of these inputs as well as the internal interpretation of the data by the equilibrium solver have uncertainties. Because of the complicated interactions of different measurements during equilibrium reconstruction, the effects of these uncertainties on the final equilibrium are not always well understood. So in order to improve equilibrium reconstruction the uncertainties in equilibria as well as their causes need to be analyzed in detail.

Chapter 2

Physical Background

In this chapter a quick overview over the physics of equilibrium reconstruction will be given. Equilibrium reconstruction is typically based on the MHD model.

2.1 Magnetohydrodynamics (MHD)

MHD describes plasmas as electrically conducting neutral fluids that are influenced by electromagnetic forces. This model is commonly used in fusion research because it describes the behavior of the plasma accurately, while still being simple enough for numerical calculations, since the plasma can be treated as one fluid instead of as individual particles [1].

2.1.1 MHD Equilibrium

In order for a plasma to be in equilibrium the balance of force between the internal plasma pressure and the magnetic field acting on the MHD fluid has to balance [2]. This leads to the equilibrium criterion for static, single fluid MHD plasmas [3]:

$$\nabla p = \mathbf{j} \times \mathbf{B} \tag{2.1}$$

where:

- $\mathbf{j}$ is the current density
- p is the kinetic pressure
- and $\mathbf{B}$ is the magnetic field.

This equation has several important implications (neglecting centrifugal forces):

- $\mathbf{B} \cdot \nabla p = 0$

  $\Rightarrow$ the pressure along magnetic field lines is constant

- $\mathbf{j} \cdot \nabla p = 0$
  $\Rightarrow$ the current flows along surfaces of constant pressure

[2]

2.1.2 Grad-Shafranov Equation

The **Grad-Shafranov equation (GSE)**: describes this balance of force for axisymmetric geometries, like the tokamak, in cylindrical coordinates. It reads:

$$R\frac{\partial}{\partial R}\frac{1}{R}\frac{\partial \Psi}{\partial R} + \frac{\partial^2 \Psi}{\partial z^2} = -\mu_0 R^2 p'(\Psi) - \mu_0^2 f(\Psi) f'(\Psi) \tag{2.2}$$

Where:

- Ψ is the poloidal magnetic flux function
- $f = \frac{\mu_0}{2\pi} I_{pol}$ is the current flux function proportional to the total poloidal current I_{pol}

[2]

2.1.3 Flux Surfaces

The Grad-Shafranov equation describes surfaces of constant magnetic flux, so called **flux surfaces**, within the plasma. These are surfaces where the flux function Ψ is constant. The magnetic field lines as well as current field lines lie on flux surfaces. Flux surfaces are typically nested in a tokamak geometry [2].

How these flux surfaces are located in a typical tokamak can be seen in Fig. 2.1. An example of different flux surfaces at ASDEX Upgrade can be seen in Fig. 2.2. These surfaces are axisymmetric around the torus.

2.1.4 Separatrix

One of the most important flux surfaces is the separatrix. It is the last closed flux surface and as such describes the border between the inner, confined region of the plasma and the outer region, where the field lines end on vessel components, the scrape-off layer (SOL). The shape of the separatrix contour reflects this. It has an important feature, called the X-point at the point in the contour where the of the low-field-side (LFS) and high-field-side (HFS) contours begin to diverge, forming a shape reminiscent of an x. This separation can be seen in the scrape-off layer contours. Within a very small region around the separatrix the behavior of the plasma as well as some key physical attributes like the temperature and density change drastically. This means that for the accurate interpretation of many measurements it is very important to know the position of the separatrix as precisely as possible [2]. In Fig. 2.2 an example of a reconstructed separatrix (blue) compared to the other flux surfaces (red) at ASDEX Upgrade can be seen.

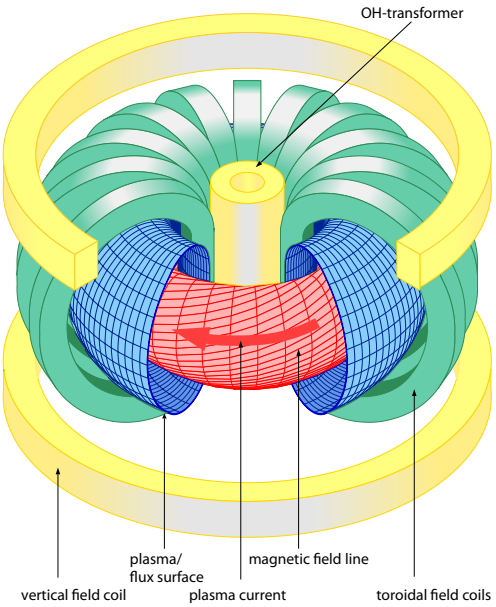

FIGURE 2.1: Flux surfaces(red) and the field coil system used to confine the plasma 3.2.1 in a typical tokamak [4]

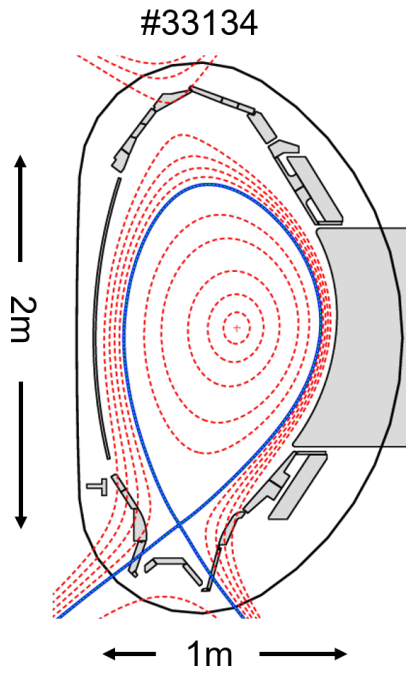

FIGURE 2.2: Example of reconstructed flux surfaces including the separatrix (blue) at ASDEX Upgrade

2.2 Equilibrium Solvers

Equilibrium solvers are codes designed to calculate MHD equilibria in fusion research. Their main components are Grad-Shafranov solvers.

2.2.1 Grad-Shafranov Solvers

As was mentioned in sections 2.1.3 and 2.1.4 the knowledge of the location and shape of flux surfaces is very important in fusion research.

For this reason a solution to the Grad-Shafranov equation (Eq.2.2) has to be found. In general the Grad-Shafranov equation does not have an analytic solution and is solved numerically [5, 6].

2.2.2 Constraints

The quality of the reconstructed equilibrium strongly depends on the amount of measurements and their uncertainties. Often equilibria are reconstructed based on magnetic data only. Since magnetic data are only measured outside of the tokamak, this can lead to large uncertainties in the equilibrium close to the center of the plasma. In order to improve the reliability of the equilibrium reconstruction the solutions of the different time points of the Grad-Shafranov equation solver can be constrained using additional measurements described in 3 and modeling quantities [7].

2.2.2.1 Measurement Based Constraints

The equilibrium reconstruction is often based on magnetic data, but the resulting equilibrium can be constrained by additional data measured by different diagnostics. Examples of this are the pressure constraints used by the equilibrium package IDE explained in section 2.2.3. A summary of used data can be found in chapter 3.

2.2.2.2 Current Diffusion

When the Grad-Shafranov equation is solved for a given time, a snapshot of the equilibrium at that time is created. This means that reconstructing an equilibrium using only a Grad-Shafranov equation solver leads to a series of unconnected solutions for each time point. An equilibrium reconstructed in this fashion does not contain any information about the temporal evolution between the time points used in the solutions. This can lead to nonphysical behavior, like jumps in the current distribution of the plasma that would not be physically possible due to, e.g., current diffusion. In an effort to connect the individual solutions and make a physically plausible reconstructed equilibrium, nonphysical, temporal smoothing constraints can be used. But since they themselves are not based on physical processes it is preferable to substitute

them through physically motivated constraints [7]. One way of doing this is to solve the current diffusion equation (CDE):

$$\sigma_{\parallel}\frac{\partial\Psi}{\partial t} = \frac{R_0 J^2}{\mu_0\rho}\frac{\partial}{\partial\rho}\left(\frac{G_2}{J}\frac{\partial\Psi}{\partial\rho}\right) - \frac{V'}{2\pi\rho}(j_{bs} + j_{cd}) \tag{2.3}$$

.

The current diffusion equation describes the temporal evolution of the flux function and, therefore, also of the current distribution in the plasma. Solving it allows for physically motivated constraints to the solutions of the Grad-Shafranov equation at the different time points. Details can be found in [7].

2.2.3 IDE

Integrated Data analysis Equilibrium (IDE) is an equilibrium solver used at ASDEX Upgrade [7]. It combines a Grad-Shafranov equation solver with a current diffusion equation solver and uses different internal constraints in order to improve the reliability of the temporal evolution of the reconstructed equilibrium [7].

The way the Grad-Shafranov equation and current diffusion equation solver interact in IDE is as follows: the Grad-Shafranov equation solver provides an equilibrium at the previous time step. The current diffusion equation solver uses this equilibrium as a boundary constraint and the current diffusion equation is then solved until the next time step of the equilibrium calculation. The current diffusion equation solver then provides its current distribution as a constraint with uncertainty to the Grad-Shafranov equation solver when calculating the next equilibrium [8].

IDE equilibria also routinely include several internal constraints based on measurements, e.g. the pressure profiles. The diagnostics used in this process will be more closely discussed in 3. The influence these constraints have on the uncertainty of the separatrix of IDE equilibria will be analyzed in chapter 4.

The Integrated Data Analysis (IDA) [9] suite is also closely integrated into IDE [7]. It combines the measurements of different diagnostics of the same physical quantity in order to improve the accuracy of this quantity. IDE uses data from IDA as a source of reliable input quantities and for constraints, improving the reliability of resulting equilibria [7–9].

2.2.4 CLISTE

The **CLISTE** (**C**omp**L**ete **I**nterpretive **S**uite for **T**okamak **E**quilibria) equilibrium solver is the standard equilibrium solver used at ASDEX Upgrade. Unlike IDE an equilibrium reconstructed by CLISTE is generally based on magnetic data only. It can be augmented, like IDE, with pressure constraints and measurements by both the MSE (section 3.4.2) and polarimetry (section 3.4.3) diagnostics. It appears at ASDEX Upgrade in the form of the EQH equilibrium, which is the most common equilibrium used for data analysis [5].

Chapter 3

Measurements and Modeling Inputs

The quality of reconstructed equilibria depends heavily on the amount and accuracy of physical quantities they are based on. In this chapter an overview over the diagnostics whose influence on the uncertainty of the separatrix position will be discussed in chapter 4 will be given.

3.1 Magnetic Measurements

The IDE equilibrium solver uses three sources for its magnetic data acquisition: the flux loop measurements, the magnetic probe arrays and the diamagnetic flux loop measurements.

3.1.1 Flux Loop Measurements

The equilibrium solvers at ASDEX Upgrade use measurements by the flux loops for the poloidal magnetic flux input [8]. These are loops of toroidal wires surrounding the torus. The change in poloidal flux is measured by measuring their induced voltage [2].

3.1.2 Magnetic Probe Arrays

The magnetic probe arrays provide measurements of the poloidal magnetic field. ASDEX Upgrade has 5 magnetic probe arrays. They each consist of a poloidally arranged array of magnetic probes surrounding the torus located at different toroidal positions.

As an example of this setup, the probe configuration of probe array 1 is shown in Fig. 3.1. The amount and poloidal placement of the magnetic probes is different between some of the arrays. The different orientation of the probes is used to measure different components of the poloidal magnetic field.

The toroidal positions of the two arrays with currently available data is shown in Fig. 3.2.

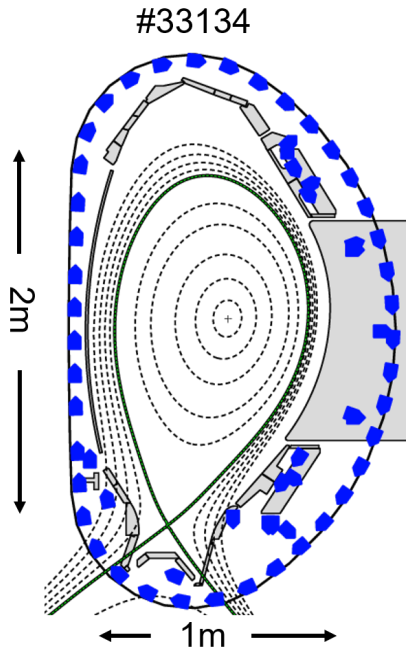

FIGURE 3.1: Poloidal view of the probe arrangement in magnetic probe array 1

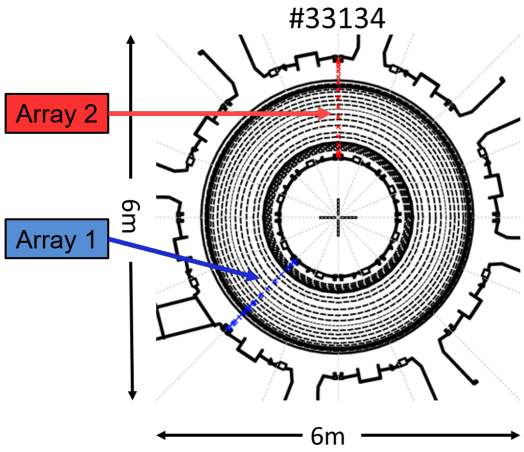

FIGURE 3.2: Toroidal positions of probe arrays 1 and 2 at ASDEX Upgrade

The different positions of the arrays means that their measurements can be used to examine the toroidal symmetry of the magnetic field. This can be used to identify local disturbances on the magnetic field as well as their influence on the calculated equilibrium [8]. Currently the data collected by only two of these arrays is readily available. Equilibria based on their data will be compared in section 4.2.1. In future experimental campaigns data from the three additional arrays will become available [10].

3.1.3 Diamagnetic Flux Loop

The diamagnetic flux loop is a set of coils designed to measure the change in toroidal flux caused by the plasma. It does this by measuring the total toroidal magnetic flux and then compensating for the toroidal flux caused by the external magnetic field [11]. IDE uses this diagnostic as an input to compare the modeled and measured diamagnetic flux [8].

3.2 Current Measurements in Poloidal Field Coils

3.2.1 Poloidal Field Coils and PSL

ASDEX Upgrade has a system of actively controlled poloidal field coils as well as a passive stabilization loop (PSL). IDE uses the current measured in the poloidal field coils as a source of constraints for the poloidal magnetic field [7]. The poloidal field coil setup (green and red) and the PSL (yellow) can be seen in Fig. 3.3.

The system of poloidal field coils is used to control the shape and position of the plasma. The coils are actively controlled during discharges and can also be used in order to calibrate the magnetic probe arrays(3.1.2) [12]. Uncertainties in this calibration process can severely influence the position of the separatrix (section 4.2.1).

The passive stabilization loop (PSL) is a system consisting of two connected, massive copper coils that are used to passively stabilize the plasma. The PSL works as follows: if changes in the magnetic field within the torus occur, (eddy) currents are induced in the PSL. This in turn induces a magnetic field which counteracts the original change. Due to this functionality, the PSL can react on a very short time scale to changes in the magnetic field. It reduces the speed of vertical drift of the plasma, counteracting so called vertical displacement events (VDEs) that can pose a risk to the machine [13].

Uncertainties on the measured currents in the PSL can, for example, be caused by local eddy currents induced in the PSL. These can be caused toroidal asymmetry in the PSL coils, like the current bridges between the upper and lower PSL. These current bridges are physical connections between the upper and lower PSL coils. To combat the negative effects of uncertainties in the measured current, the PSL current is fitted. The choice of level of uncertainty affects the position of the separatrix (section 4.3.2)

3.2.2 Currents in Vessel Components

Rapid changes in the plasma (magnetic field) can induce eddy currents in metallic vessel components. These structures are not necessarily toroidally symmetric. The induced eddy currents can induce magnetic fields and thereby distort the magnetic data input of the equilibrium solver. Unfortunately no

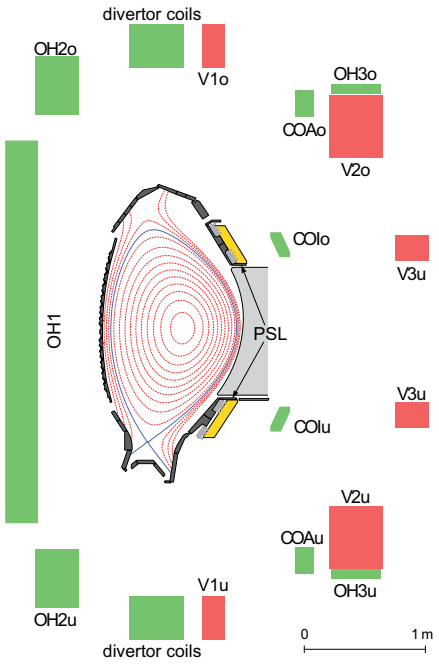

FIGURE 3.3: Poloidal field coil system at ASDEX Upgrade [14]

diagnostic or modeling is available to determine the asymmetries caused by such eddy currents. In an effort to counter their influence on the equilibrium IDE as well as CLISTE allows for user defined variability (uncertainty) in the poloidal-field coil currents. This flexibility in the coil currents allows improved fits of the magnetic data, especially in the current ramp-up and ramp-down phases and has an influence on the position of the separatrix.

3.3 Pressure Measurements

The pressure is one part of the force balance of the MHD equilibrium. IDE uses three partial pressures to model the total pressure: The thermal electron pressure p_e, the thermal ion pressure p_i and the fast-ion pressure p_{fast} caused by the Neutral Beam Injection (NBI) heating system [7, 15]. The data acquisition for each of these partial pressure contributions is different and subject to different uncertainties [8].

3.3.1 Thermal Electron Pressure

The IDE equilibrium solver uses data from the IDA framework [9] for its measurements of electron temperature T_e and density n_e, which make up the thermal electron pressure [8].

IDA is based on the combination of different diagnostics to measure different physical quantities:

- electron cyclotron emission (ECE) diagnostic measures T_e at the low-field-side (LFS) midplane from the plasma core to the edge
- lithium beam emission spectroscopy (LiB) diagnostic measures n_e on the upper LFS at the plasma edge
- interferometry measures the line integrated n_e on 5 lines of sight (LOS) above the midplane
- Thomson scattering (TS) diagnostic [16] measures n_e and T_e with two vertical systems:
  - core TS system measures at the lower part of the LFS and into the core of the plasma
  - edge TS system measures at the LFS midplane close to the separatrix

The combination of these measurements are combined by IDA to generate more accurate profiles. The quality of the output profiles depends on the amount of available diagnostics with reliable data for each physical quantity in the analyzed discharge [9].

3.3.2 Thermal Ion Pressure

The ion temperature T_i used by IDE is obtained through the Charge eXchange Recombination Spectroscopy diagnostic (CXRS). It works on the principle of the measurement of emitted characteristic line radiation during the transfer of electrons from a beam of neutral particles to impurity ions in the plasma [17, 18]. CXRS profiles at ASDEX Upgrade are only provided for discharges where the plasma is heated via NBI [17]. The sight lines of the CXRS diagnostic are located directly next to the two NBI boxes at ASDEX Upgrade.

If no CXRS measurements are available, IDE assumes either $T_i = T_e$ or an empirical relation for ohmic discharges [19]. This is not always accurate however. The electron temperature can be influenced by Electron Cyclotron Resonance Heating (ECRH) [8]. This is a system used for heating plasmas based on microwave radiation accelerating electron cyclotron motion [2]. This means that when only the ECRH is used, the electron temperature is influenced while the ion temperature is only influenced indirectly via heat exchange [2]. This means that the assumption $T_i = T_e$ is no longer accurate. Analogously if Ion Cyclotron Resonance Heating (ICRH) is used mainly the ion temperature is influenced [8].

The thermal ion density n_i is provided to IDE by a combination of the electron density from IDA, from which the fast-ion density is subtracted and the Z_{eff} profile. The effective charge provides an estimation of the ratio of

ions to electrons in the plasma. Z_{eff} can be obtained through a combination of bremsstrahlung or the CXRS impurity profiles [8, 20, 21].

3.3.3 Fast-Ion Pressure

Fast ions produced by the NBI also have an impact on the plasma and the reconstructed equilibrium. They have a low density, but very high energy and so are able to influence the total pressure of the plasma quite significantly. This means that the fast-ion pressure can have a significant impact on the equilibrium reconstruction of discharges heated by NBI. The sensitivity to this influence is analyzed in section 4.5. Very recently the newly developed RABBIT code [15] has been implemented into IDE as the primary source of fast-ion pressure input [19]. In section 4.5 the difference between equilibria based on RABBIT profiles and those based on the previously used TRANSP code will be evaluated.

3.3.4 Total Pressure

When all partial pressures have been obtained, they can be added up to obtain the total pressure, where the temperatures used are in eV:

$$p_{tot} = (T_e\, n_e + T_i\, n_i) + p_{fast} \tag{3.1}$$

3.4 Current Distribution Measurements and Modeling

As mentioned in 3.4.4 the current diffusion equation can be solved to provide a physically motivated evolution of the current distribution in between time points for which the Grad-Shafranov equation is solved. Additionally, measurements of the current distribution can be used to constrain the solution of the Grad Shafranov solver [7, 8]. By using measurements or modeling(section 3.4.4) of the current distribution as constraints, a more accurate solution to the Grad-Shafranov equation can be found. This improvement is especially important in the center of the plasma, often providing a large influence on the location and shape of the inner flux surfaces [7]. There are 4 different diagnostics used by IDE with which the internal current distribution of the plasma can be measured: tile currents, the Motional Stark Effect (MSE), imaging MSE (iMSE) and the polarimetry diagnostics. The temporal evolution of the current distribution is described by the current diffusion equation solver discussed in section 3.4.4.

3.4.1 Tile Currents

IDE and CLISTE use the measurement of currents on the divertor tiles as constraints to the current profile in the SOL [7]. Uncertainties in the current

in the SOL can strongly influence the position of the separatrix, especially the position of the X-point. A sensitivity study of this phenomenon will be discussed in section 4.4.

3.4.2 MSE and iMSE

If available, IDE uses data from the MSE or iMSE system to constrain the current density profile. The MSE diagnostic measures the polarization of the Balmer α line emission of an injected neutral hydrogen or deuterium beam [22, 23]. The imaging MSE (iMSE) diagnostic is based on the same principle, but uses modern equipment to improve the signal-to-noise ratio and the amount of data collected by the system drastically [23]. MSE data provides spacial information about the current distribution. The spacial resolution of MSE is, however, not high enough to provide well-posed constraints for the equilibrium reconstruction [7]. Unfortunately the MSE/iMSE diagnostics are not available during a majority of discharges and their calibration can be challenging [7, 8].

3.4.3 Polarimetry

The polarimetry diagnostic works by measuring the polarization of a laser beam that has gone through a plasma and has had its polarization altered by Faraday rotation [24]. Polarimetry data is commonly available and can be used for information on the current distribution, but is based on line-integrated measurements. Since only two lines of sight are equipped with polarimatry measurements the spacial resolution is poor [7].

3.4.4 Current Diffusion Modeling

As mentioned in section 3.4.4 IDE also models the current density profile using a current diffusion equation solver. The uncertainty of the solution of the current diffusion equation solver needs to be estimated and adjusted for different plasma scenarios. Typically in IDE a relative uncertainty of 10% as well as an absolute uncertainty of $2 \cdot 10^5\,\mathrm{Am}^{-2}$ are assumed.

Chapter 4

Sensitivity Study on Separatrix Position

In chapter 3 an overview over measurements and modeling inputs used by IDE was given. Changing these input parameters as well as what constraints are based on them during reconstruction can influence the position of the separatrix to varying degrees. The differences in the position of the separatrix associated with some of these different influences will be discussed in this chapter.

Fig. 4.1 shows an example of two different separatrix contours (blue and violet). Some important locations on the contour are marked here, like the X-point, the midplane on the low-field side and the point where the core Thomson scattering diagnostic intersects with the separatrix contour. These features are marked using the poloidal angle with $R_0 = 1.65\,\mathrm{m}$ as a fix point.

In this example the blue separatrix was calculated using constraints with uncertainties to fit the currents of all poloidal field coils. The magenta separatrix belongs to an equilibrium based on the raw measured poloidal field coil currents. In this case the difference between the two separatrices can be seen even when looking at the entire separatrix contour. This means the difference between the two separatrices is quite significant.

The profile of the distance between the violet and blue contour of this example over the whole poloidal angle can be seen in Fig. 4.2. The separatrix based on raw current data is about 14 mm further outwards on the high-field side close to the X-point than the one based on fitted current data. These difference profiles were calculated by measuring the distance of each point on the first separatrix contour to the second contour, then averaging this distance for all points within the same degree of poloidal angle and finally averaging all the points assigned to each degree over the time ranges listed in table 1. The result of this analysis is then a profile of the difference between two separatrices as seen in Fig. 4.2. A positive distance means that the second separatrix is positioned further away from the magnetic axis at a given point on the contour when compared to the baseline separatrix. A negative value means the second separatrix is positioned closer to the plasma core than the

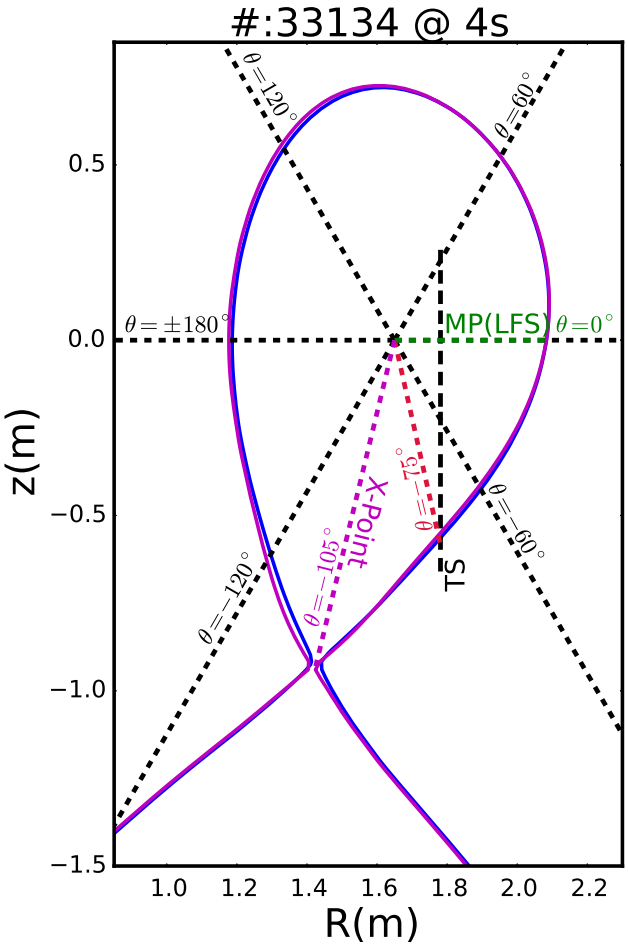

FIGURE 4.1: Different separatrix contours with and without poloidal field coil current fitting

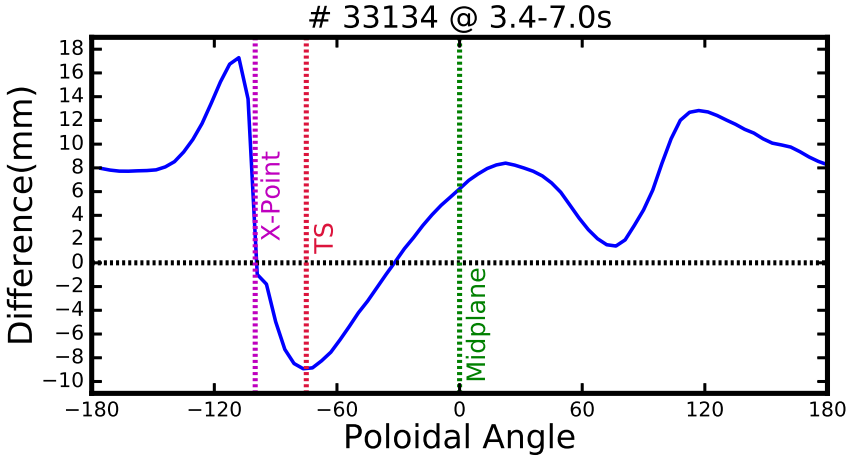

FIGURE 4.2: #33134 Difference between separatrices of Fig. 4.1 over the poloidal angle

baseline separatrix. The settings used in the reconstruction of the baseline equilibria is discussed in section 4.6. In all equilibria where an analysis of the edge-localized modes times was available, the time points between 0.7 ms before and 2 ms after the maximum power load of an edge-localized mode onto the divertor were excluded.

4.1 Scenarios

The discharges selected for analysis were based on the already publicly available IDE equilibria starting at discharge #33000 which were originally available at the time the thesis was started. This group was expanded when during an analysis one discharge produced especially interesting results, by adding discharges similar to it. One ohmic discharge (#33692) was originally used in the beginning of the work on this thesis to understand differences in equilibrium reconstruction in a less complex scenario. By analyzing the ohmic discharge, it was seen that IDE and CLISTE produce very similar equilibria in low-energy scenarios and the focus was shifted to H-mode equilibria. In total 45 discharges were used for the analysis. They are listed together with their plasma parameters in Table 1 in Appendix A.

In each of the sensitivity studies in the sections of this chapter discharge #33134 was used as a baseline scenario. This discharge was intensively studied with IDE [25] and was the only discharge with all of the diagnostics used by IDE available. After this, as many of the remaining discharges in the pool were used as possible to get the most accurate estimation of the sensitivity.

4.2 Magnetic Measurements

4.2.1 Magnetic Probe Arrays

As discussed in section 3.2.1 the magnetic probe arrays are the basis of the poloidal magnetic field used by IDE. This means that their uncertainties can have a major influence on the separatrix position. To quantify the differences caused by the data from the different probe arrays, two equilibria were calculated for a large number of discharges in this study. One of these equilibria was based on data from probe array 1 and one on data from probe array 2. Probe array 1 was used for the baseline equilibria against which the equilibria based on magnetic data from array 2 were compared.

As can be seen in Fig 4.3 the typical difference between separatrices based on the two arrays is quite substantial. This difference typically ranges between 5 – 10 mm at the X-point and between 2 – 6 mm at the midplane.

The shape of this profile is the same for every shot examined. This holds true for all scenarios examined in this work. When comparing these two separatrices one can see that the separatrix based on the first field coil is positioned

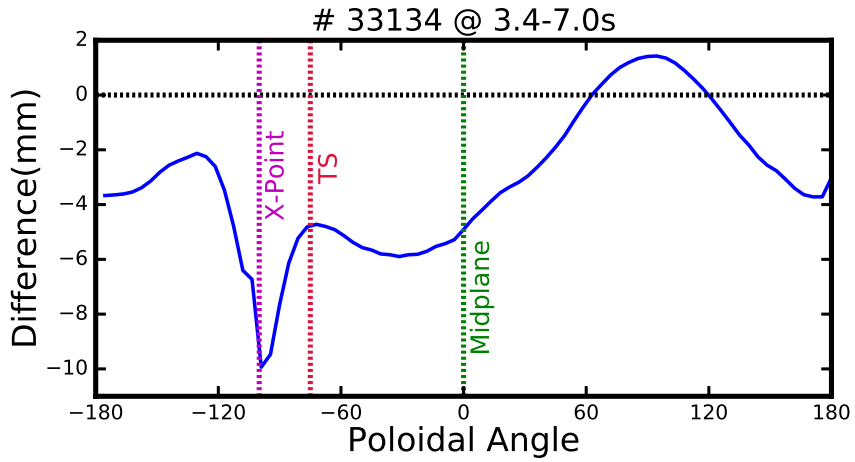

FIGURE 4.3: Typical difference profile using different magnetic probe arrays

further outwards than that of the second field coil on the entire lower half of the plasma. An example of this can be seen in Fig. 4.4.

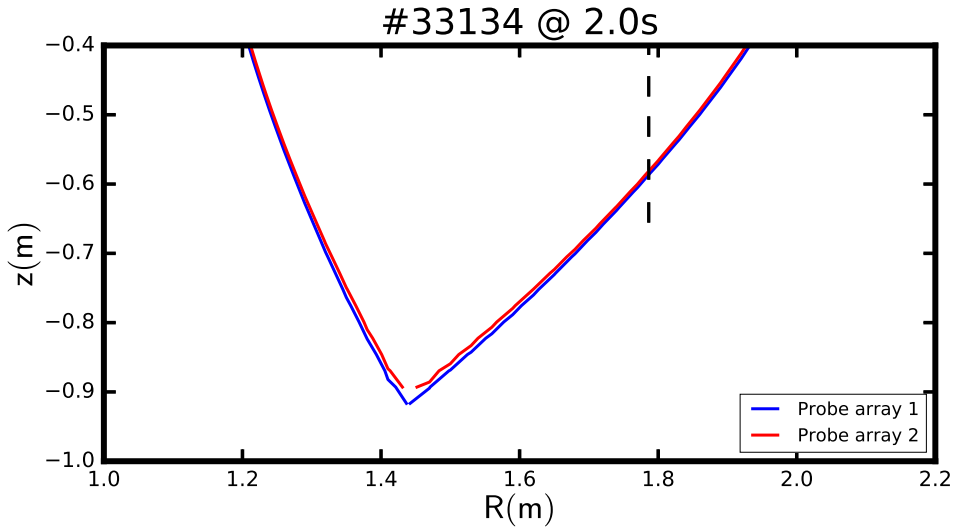

FIGURE 4.4: Typical example of separatrix contours based on probe array 1 and 2

The first idea for the explanation of this phenomenon was that an uncertainty in the location of the different probe arrays could lead to a shift in the location attributed to the magnetic measurements, which in turn could cause a difference in the separatrix position. To analyze this idea, a study was conducted, where equilibria were reconstructed with artificially spatially shifted magnetic data. It was later discovered, however, that the separatrix based on data from array 2 was moved inwards (towards the magnetic axis) on both the high-field side and the low-field side. This made the explanation based on spacial uncertainty implausible, because in the case of the spacial uncertainty, a difference in the same radial direction for both parts of the contour would be expected.

This means one would expect the equilibrium based on array 2 to have a lower total volume inside the separatrix than the plasma based on array 1. This can be seen in a time trace in Fig. 4.5. The cause of this phenomenon is a lower toroidal plasma current measured by coil 2 than that measured by coil 1, as shown in Fig. 4.6.

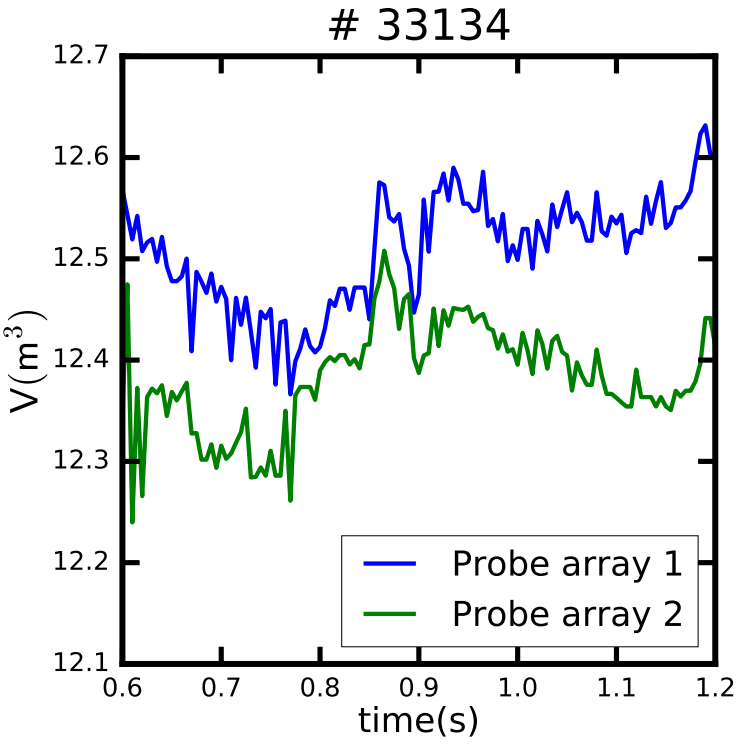

FIGURE 4.5: Plasma volume within separatrices based on different arrays

The reason for this seems to be the calibration technique used to calibrate the probe arrays. During calibration, a current is applied to the poloidal field coils without plasma and the response of the probes to the known magnetic field is then used to calibrate them [12]. The calibration is accurate to about 1% [12]. This matches nicely with the result seen in Fig. 4.6 where a difference of 1% between the total currents can be seen. Therefore, although the calibration uncertainty is rather small, it has a major effect on the position of the separatrix.

In this study discharges from 2015 to 2017 were analyzed. The difference in separatrix position has had the same shape since the second coil array was installed. A calibration of the probe arrays has been conducted multiple times in this time frame [12]. This means that the calibration seems to have a very similar uncertainty every time it is conducted.

Concluding, the uncertainty in the calibration of the poloidal coil arrays leads to a typical uncertainty of the separatrix of about 7 mm at the X-point and 5 mm around the lower half of the contour. Currently data is only available from two probe arrays. This means that it is not possible to know which of

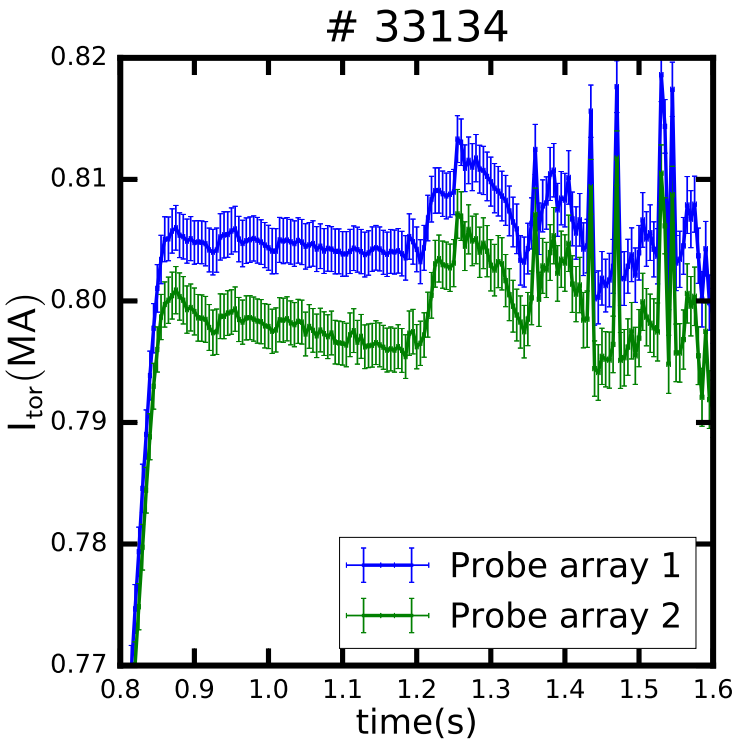

FIGURE 4.6: Toroidal plasma current with uncertainties of equilibria based on different arrays

the two coil arrays measures a more accurate magnetic field. This discrepancy is expected to be resolved when the probe arrays 3 – 5 provide measurements in future campaigns. IDE as well as CLISTE use array 1 as a basis for their standard reconstruction. Since it is unknown if array 1 produces a more accurate magnetic field, this could mean an uncertainty in the position of the separatrix in all discharges for both equilibrium solvers.

4.2.2 Magnetic Data Preprocessing

Another way to influence the position of the separatrix is to change the preprocessing of the magnetic data used by the equilibrium solver. The preprocessing settings influence the background subtraction and toroidal field correction used on the raw magnetic data. In an attempt to understand the differences between the IDE and the CLISTE equilibria, the identical magnetic data preprocessing used by CLISTE was also used in IDE. The resulting differences in separatrix position of the standard CLISTE equilibrium compared to IDE separatrices based on the typical preprocessing settings used to reconstruct IDE equilibria(blue) and on the same preprocessing as CLISTE (green), respectively, can be seen in Fig. 4.7.

The typical difference profile between the CLISTE separatrix and that of IDE using standard magnetic preprocessing can be seen in the blue line. The strongest discrepancy between the two different equilibrium solvers is near the

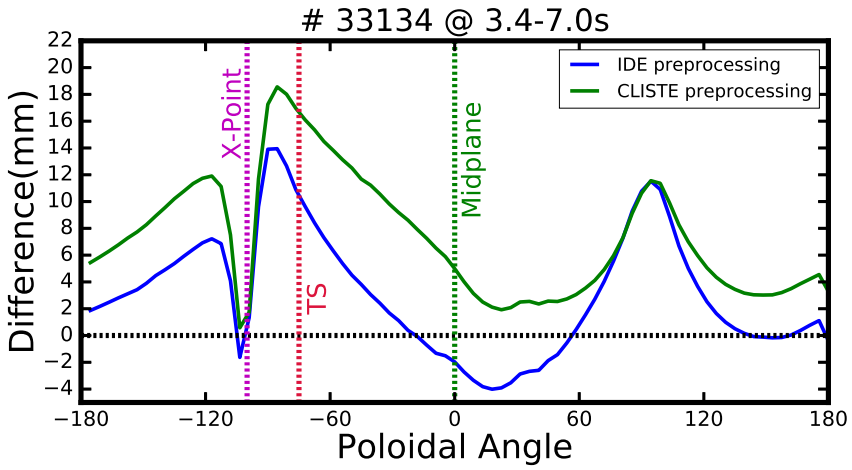

FIGURE 4.7: Difference between separatrices of the standard CLISTE equilibrium and IDE equilibria using standard magnetic data (blue) and the same preprocessed magnetic data as CLISTE (green)

X-point and on the very top of the contour. This difference is typically 10 mm.

The green line shows the difference between the two separatrices when using the same magnetic preprocessing on the IDE data that is used in CLISTE equilibria and comparing it to the same CLISTE equilibrium as in the blue line. The difference at the upper part of the separatrix contour stays the same, while at the same time the difference across the remaining part of the separatrix is increased by an almost constant amount. This means that the IDE separatrix stays constant on top of the contour and is shifted outwards by approximately 4 mm everywhere else using the same magnetic data as CLISTE. Therefore the difference between the IDE and the CLISTE equilibria is not caused by the different magnetic data preprocessing settings, but to the larger amount of information used by IDE, e.g. current diffusion, pressure constraints, etc.

4.3 Poloidal Field Coil Current Measurents

4.3.1 Variability of Current in V-Coils

In this section a close look will be taken at the influence of the poloidal field coils on the separatrix contour. The currents measured in the different poloidal field coils are used to calculate the magnetic field caused by the coils as well as for constraints to the equilibrium. The influence of the V-coils is analyzed in this section. These are the coils: V1o, V1u, V2o, V2o, V3o and V3u. They are marked in red in Fig. 3.3. For a large pool of discharges, one equilibrium was calculated using an allowed variability of 500 A and one using 50 A to the measured current of each of these coils, with the variability setting of 500 A being used for the baseline equilibria. Allowing a higher variability in the current allows the equilibrium solver the possibility of modeling a current that

has a higher difference to the one measured in the coil while trying to minimize the difference of the measured and modeled data.

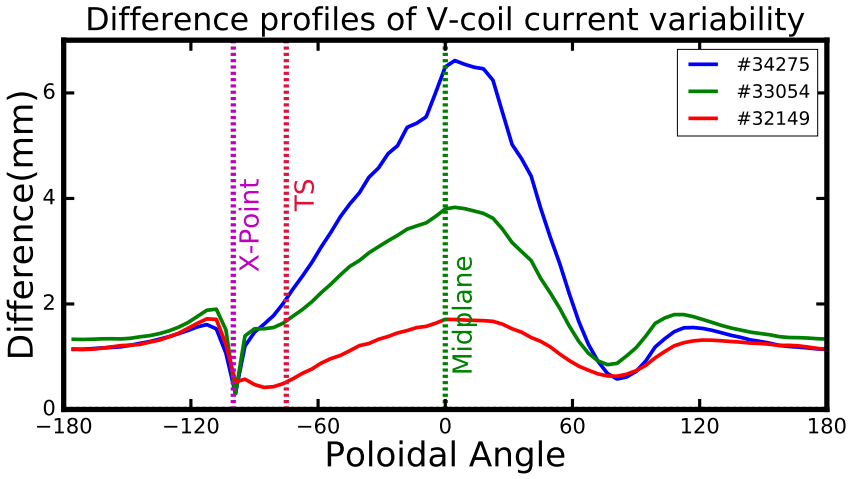

FIGURE 4.8: Difference profiles of current variability in V-coils

As examples of the influence of this effect, the difference profiles are shown for discharges #32149, #33054 and #34275 in Fig. 4.8. The shape of the difference profile is very similar for all discharges used in this examination. The difference caused by the different current constraints is most apparent at the midplane on the low-field side and can vary between 2 – 10 mm for all discharges examined. The uncertainty also affects the entire high-field side contour. This is a much smaller effect, typically between 1 – 2 mm for all shots. The high-field side contour does not seem to be affected very much by current uncertainties. This is most likely caused by the fact that most of the V-coils are positioned around the LFS of the vessel.

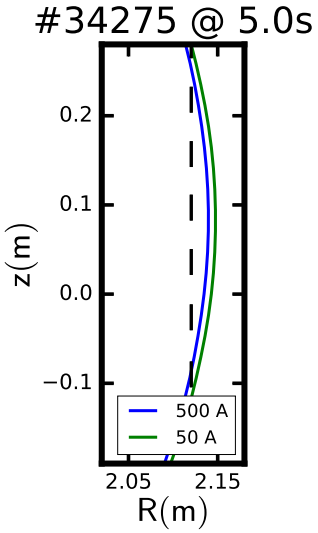

FIGURE 4.9: Separatrix contours with different allowed V-coil current variability

An example of the position of the different separatrix contours around the midplane can be seen in Fig. 4.9. The separatrix based on the higher allowed variability in the currents is mapped further inwards, whereas the separatrix based on the lower allowed variability is mapped further outwards. The different separatrix contours of #34275 will be closely examined in sections 5.2.2 to 5.2.4, where a validation study will be conducted using different techniques to decide which of the allowed current variabilities leads to a more reliable separatrix reconstruction at the LFS midplane. This variability study will lead to the decision to use the 500 A allowed variability as a standard setting for the equilibria used in this thesis. The equilibrium using the lower amount of allowed variability in the V-coil currents very closely resembles the position of the CLISTE equilibrium at the midplane. This can be used to create an IDE equilibrium that can be compared closely to CLISTE in this region.

4.3.2 Variability of Current in PSL

Another major influence on the separatrix position is caused by the current in the passive stabilization loop (PSL). The two PSL coils are marked in yellow in Fig. 3.3. The PSL is inside the vessel, close to the plasma and can have a very direct and local influence on the plasma shape. To analyze the influence of the PSL on the equilibrium, equilibria based on the raw measured currents in the upper and lower PSL were compared to equilibria using fitted currents.

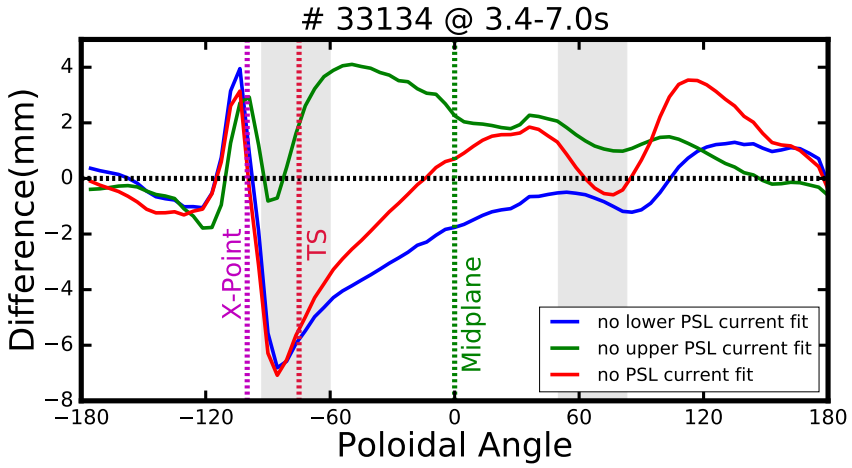

FIGURE 4.10: Contour difference of PSL current fit, areas close to the two PSL coils are marked in gray

4.3.2.1 Influence of the Upper PSL

Typically a variability of 1 kA is allowed for the fit of the current in the upper PSL. Equilibria were calculated not allowing this fit and instead using the measured current in the PSL. A typical example of the difference profile between this equilibrium and one using the 1 kA variability can be seen as the

green line in Fig. 4.10. Disabling the fit of the current in the upper PSL shifts the separatrix position outwards over the contour starting at the lower PSL and ending on the side opposite the upper PSL. This behavior indicates that the fitted current in the lower PSL is influenced by the setting of the current in the upper PSL.

4.3.2.2 Influence of the Lower PSL

Analogously the fit of the current in the lower PSL was disabled, using the measured current instead of the modeled current with the typically allowed variability of 0.5 kA. The result can be seen in the blue line of Fig. 4.10. The separatrix position shifts inwards by about 6 mm at the point where the lower PSL is closest to the plasma in the case shown here, but this difference can vary quite significantly between scenarios. The shots analyzed in this study showed behaviors ranging from an inwards shift of up to 8 mm (#33379) to an outwards shift of 2 mm (#33173). The exact cause of this strong divergence is currently not known, but the inwards shift seems to increase with an increase in the amount of NBI heating. The effect of the lower PSL fit influences the separatrix position to about the point at which the upper PSL comes closest to the plasma.

4.3.2.3 Influence of Both PSLs

Finally a study was conducted using the measured data of both PSL coils. Typical results of this can be seen in the red line of Fig. 4.10. Disabling the current fit in both PSLs simultaneously leads to a difference profile that seems to be a weighted combination of the difference profiles of the individual PSL coils. Interestingly, close to the lower PSL, the combined difference profile closely resembles that of the current in the lower PSL. In the rest of the contour the combined difference profiles is weighted between the two individual difference profiles.

The PSL sensitivity study was particularly interesting during the uncertainty estimation of the core TS diagnostic, which will be discussed in section 5.2.1.

4.3.3 Fit of all Currents

In sections 4.3.1 and 4.3.2 the influence of the V-coils as well as the PSL on the separatrix contour were discussed. These are two sets of coils that have a large impact on the location of the separatrix contour. In this section the combined influence of the fit to the current in all poloidal field coils will be analyzed.

The influence the current fit of all coils has on the separatrix position can be seen for three examples in Fig. 4.11. In the analysis of the larger pool of discharges, all discharges seemed to fall into the two shape archetypes represented by #33616 and the other two discharges, respectively. One, like

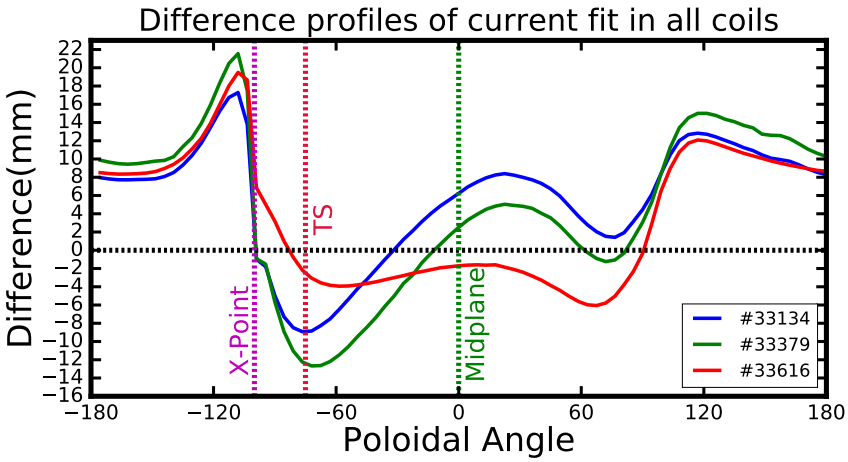

FIGURE 4.11: Uncertainty of current fitting of all coils

the one of #33616, where the separatrix based on the measured currents in the coils is positioned further inwards to almost the same magnitude at the point, where the core Thomson diagnostic intersects with the separatrix contour and at around 70°, while staying shifted inwards in between. The other archetype, represented here by #33134 and #33379 has a strong inwards shift at the core TS diagnostic, and then is shifted outwards at around the midplane. It is currently not clear why the discharges are divided into these two distinct groups, but typically discharges with lower heating fall into the first archetype, while discharges with higher heating adhere to the second archetype.

In the difference profile, the influence of the current fit of the individual coils can also be seen. This is especially evident when looking at the difference profile of #33134 and comparing it to the difference contour linked to the disabled fit of the PSL current shown in Fig. 4.10 as the red line. The shape of the uncertainty contour is very similar in both cases. This means the PSL current has a very large influence on the contour, which makes the exact knowledge of its current especially important, because uncertainties can have such a large impact on the total contour.

It is also interesting that the difference profile shape of #33134 and #33379 between the X-point and the top of the separatrix at around 100° looks very similar, while being shifted by an almost constant amount and changing sign at different times. This can be explained partially by effects on a short time scale, such as edge-localized modes (ELMs). In Fig. 4.12 the time trace of the difference at 70° between $3.5 - 4\,\mathrm{s}$ is shown. The blue line shows the difference at all time points of the calculated equilibrium. The green line shows the time points remaining after excluding ELMs. To exclude ELMs all time points between 0.7 ms before and 2 ms after the maximum power load onto the divertor caused by an ELM were excluded, as discussed in the introduction of this chapter. In Fig. 4.12 it can be seen, that the time points close to ELMs generally have a stronger inwards shift than the time points outside of the influence of ELMs. Because of this, a difference profile using all time points

will be shifted to lower numbers, than one using only time points not close to ELMs. This can be seen in Fig.4.13.

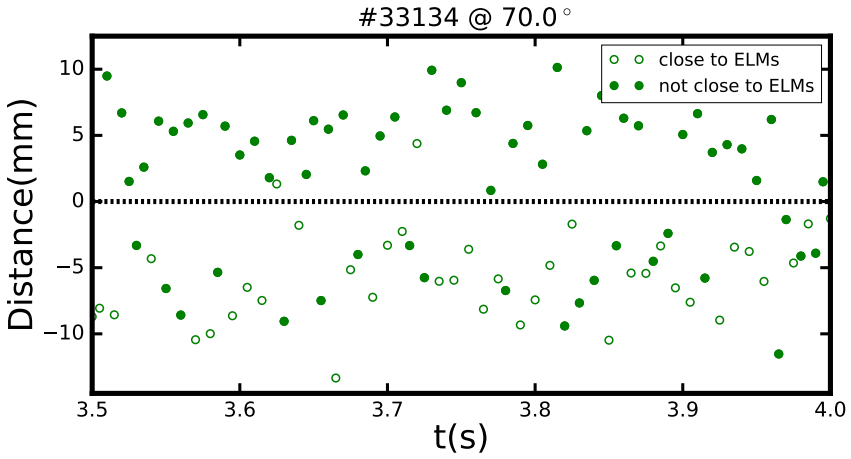

FIGURE 4.12: time trace of the difference profile at 70°. Filled in dots are calculated at times outside the influence of ELMs, empty dots are close to ELMs.

Here the same difference profiles as depicted in Fig. 4.11 are shown (solid lines) as well as those same difference profiles including the time points close to ELMs. Discharge #33616 is not depicted here, because it has no available ELM analysis. If the time points close to ELMs are included, a shift of the difference profile towards lower values can be observed in all parts of the separatrix contour except between the X-point and the point in the contour where the core Thomson scattering diagnostic intersects with the contour.

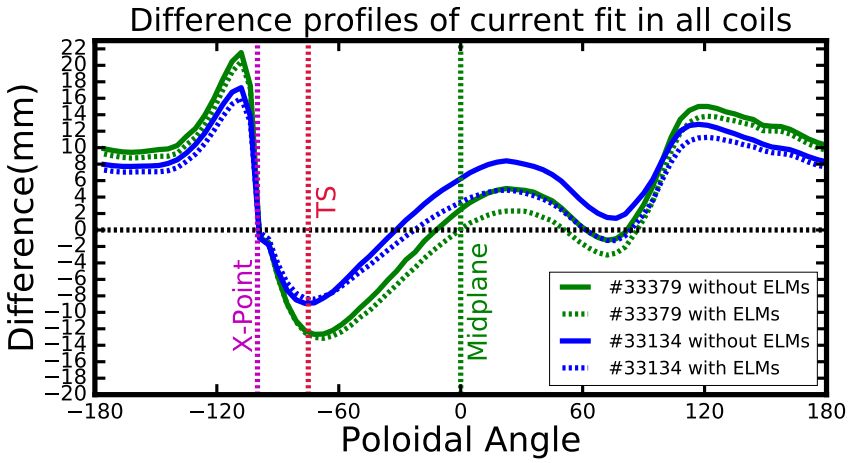

FIGURE 4.13: Uncertainty of current fitting of all coils

ELMs were used here as an example on how phenomena on a short time scale can influence the difference profile. This phenomenon is important to the sensitivity study on the effects of the current fits in the poloidal field coils, because as discussed in section 3.2.2 these phenomena can induce eddy currents

within vessel components. The larger allowed variability helps the equilibrium solver to counteract the influence of these eddy currents on the magnetic field and in turn on the measured current in the poloidal field coils. This means that equilibria not using current fits or very low allowed variability in the coil currents are more susceptible to the influence of these short term phenomena.

4.4 Scrape-off Layer Current

In this chapter the uncertainty caused by a lack of modeling of the SOL current distribution will be discussed. Typically IDE models the scrape-off layer currents out to a normalized radius of $\rho_{pol} = 1.02$. For this analysis equilibria were written only modeling the current distribution until the separatrix at $\rho_{pol} = 1$. In Fig. 4.14 a typical uncertainty profile of this effect can be seen.

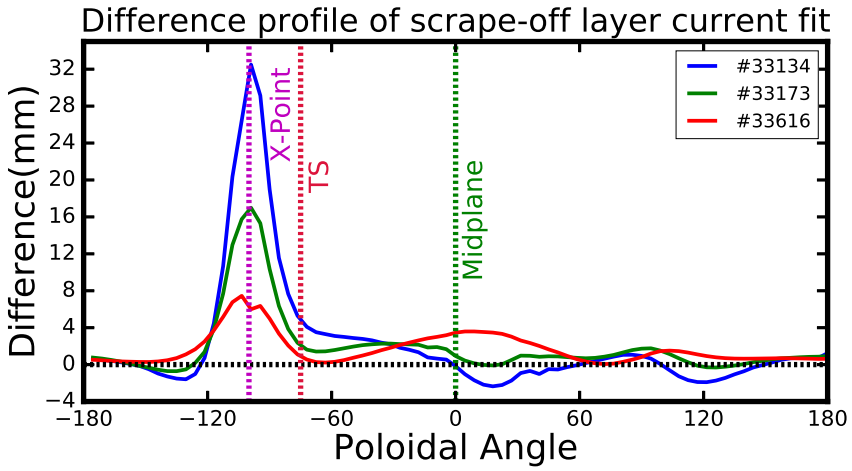

FIGURE 4.14: Difference profile of SOL current modeling

The separatrix position is most strongly influenced around the X-point with uncertainties of up to 4.5 cm. With the X-point of the equilibria not using scrape-off layer current modeling being shifted downwards. The rest of the separatrix contour is also influenced but on the order of 2 mm only.

4.5 Sensitivity to Missing fast-ion Modeling

As discussed in section 3.3.3 the fast-ion modeling influences the separatrix in discharges using neutral beam heating. To quantify this effect a sensitivity study was conducted. Equilibria without fast-ion modeling were compared to the base equilibria, those using fast-ion modeling.

The effects on the separatrix contour can be seen in Fig. 4.15. As an example of the results of this analysis three discharges will be compared with different NBI power and plasma current. These can be seen in table 4.1.

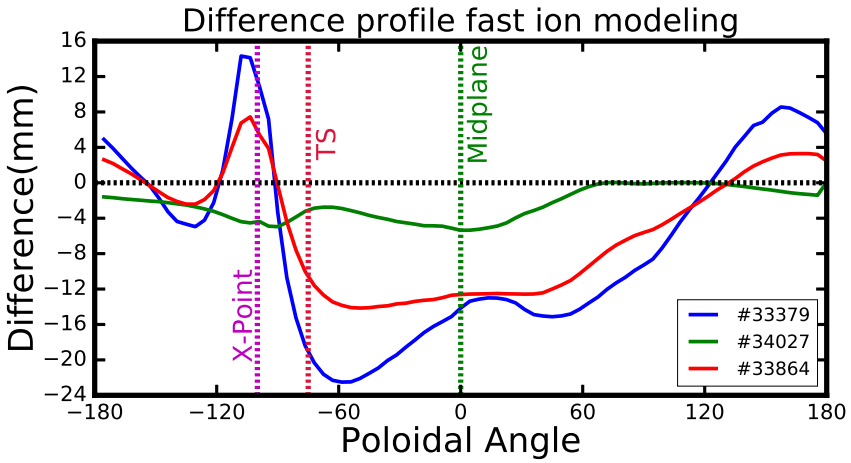

FIGURE 4.15: Difference in separatrix contours caused by fast-ion modeling

#	$P(NBI)$	I_p
33379	14.4 MW	0.6 MA
33864	15.0 MW	0.8 MA
34027	6.7 MW	0.8 MA

TABLE 4.1: Plasma parameters of discharges in Fig. 4.15

The difference measured at the mid-plane changes with the total amount of NBI power used during discharges. In Fig. 4.15 the difference profiles of these different scenarios can be seen. In general there is an inwards shift of the separatrix not using fast-ion modeling on the low-field side. At the X-point an outwards shift can be observed for the two discharges with higher NBI power (#33379 and #33864) while a slight inwards shift is seen for the discharge with less heating (#34027). A large difference in the magnitude of the uncertainty at the midplane can be seen between #34027 and the other two discharges.

When comparing #33379 and #33864 which both have a similar amount of neutral beam heating, the difference at the midplane stays consistent, while the shape of the difference profile changes considerably. This is especially apparent close to the point, where the core TS diagnostic intersects with the separatrix contour and at around 60°. One difference between the two discharges is, that #33379 has a plasma current of $I_p = 0.6$ MA while #33864 has an I_p of 0.8 MA. This change in shape can be seen consistently when comparing discharges with the same NBI power but different I_p.

Additionally the influence the simplifications of the newly implemented RABBIT code have on the calculated equilibrium was examined for one shot. A separatrix based on fast-ion pressure calculated by the RABBIT code was compared to one based on the previously used TRANSP code. The uncertainty was less than 0.5 mm over the entire contour, which is negligible.

4.6 Baseline Equilibrium

In each of the sensitivity studies some of the input settings or parameters typically used in IDE equilibria were changed to reconstruct comparison equilibria. These comparison equilibria were then compared to baseline equilibria of the same discharge. Baseline equilibria were calculated with the same settings for each of the discharges used unless certain diagnostics such as the motional Stark effect diagnostic were unavailable. In this case all other settings were kept the same and the unavailable diagnostics excluded from the reconstruction. The different input parameters on which the baseline equilibria were based are listed in table 4.2. All other input parameters in the equilibrium were set to the typical settings used in standard IDE equilibria. Also listed are the same input parameters used in the comparison equilibria in the different sensitivity studies.

Input parameter	baseline	comparison	section
mag. probe array	Array 1	Array 2	4.2.1
var. V-coil curr.	500 A	50 A	4.3.1
PSL curr. fit	yes	no	4.3.2
pol. field coil curr. fit	yes	no	4.3.3
SOL current fit	yes	no	4.4
Fast ion modeling	yes	no	4.5

TABLE 4.2: Input parameters used to reconstruct the baseline equilibrium

4.7 Summary of the Sensitivity study

In this section an overview of the various differences discussed in the previous chapter will be given. In table 4.3 the typical differences found in the various sensitivity studies are shown. A positive number means the separatrix contour influenced by the effect analyzed in the given sensitivity study or comparison separatrix is moved outwards when compared to the baseline separatrix. A negative value means that the comparison separatrix is moved inwards towards the center of the plasma at this point. The abbreviations used in the first column are the same used in table 1 in Appendix A. The values shown in table 4.3 depict the typical difference observed, but this value can vary quite significantly in some cases like in the sensitivity study over the influence of the current fit of all coils.

In the Probe array study (PA, section 4.2.1) poloidal magnetic fields from different magnetic probe arrays were used to construct equilibria. This phenomenon affects primarily the lower part of the contour and causes a shift inwards for equilibria based on the second probe array, resulting from a lower toroidal plasma current and leading to a reduction of the plasma volume.

source	mp LFS	TS Core	X-point	mp HFS	Top of contour	section
PA	−4 mm	−3 mm	−7 mm	−3 mm	1 mm	4.2.1
V	4 mm	2 mm	1 mm	1 mm	1 mm	4.3.1
PSL	2 mm	−1 mm	0 mm	−1 mm	−2 mm	4.3.2
CF	1 mm	−4 mm	0 mm	6 mm	10 mm	4.3.3
SOL	1 mm	3 mm	15 mm	1 mm	2 mm	4.4
FI	−8 mm	−8 mm	4 mm	1 mm	−6 mm	4.5

TABLE 4.3: Typical differences of the separatrix contour caused by the different influences discussed in chapter 4

In the V-coil sensitivity study (V, section 4.3.1) the allowed variability in the current measured in the V-coils was reduced from 500 A to 50 A. This led to an outwards shift primarily around the midplane on the low-field side.

During the study on the effects of the PSL current (PSL, section 4.3.2) the fit of the PSL currents was disabled. An inwards shift was observed close to the two coils. The magnitude of which varies widely between shots close to the lower PSL.

The study on the effects of a disabled current fit of all coils (CF, section 4.3.3) showed two distinct groups of difference profiles. The first group of discharges showed an inwards shift along the entire low field side in the equilibria with a disabled current fit, while the other group showed an inwards shift beginning at the midplane on the low-field side.

The effects of disabling the modeling of the scrape-off layer current (SOL, section 4.4) could be seen primarily in a strong downwards shift of the X-point in equilibria with the disabled modeling.

Another study was conducted, where the fit of the fast-ion pressure was disabled(FI, section 4.5). The equilibria affected by this change showed an inwards shift on the entire low-field side. The magnitude and shape of this shift seemed to vary depending on the amount of neutral beam heating during the discharge, as well as the plasma current.

More in-depth discussions of the individual studies can be found in their respective sections.

Chapter 5

Validation

As discussed in chapter 4 the separatrix position can be influenced by a large number of different factors. To be able to use this information, it is important to be able to analyze the reliability of the different separatrix contours. In this chapter different validation techniques will be discussed and used to validate different parts of the separatrix contour.

5.1 Scenarios

The validation techniques each have individual challenges associated with their shot selection. The Thomson scattering based validation technique (section 5.2.2) relies on the position of the separatrix relative to the Thomson channels. For the two-point model validation (section 5.2.3) and the strike point validation (section 5.3), the measurements of each time point had to be evaluated by hand by Martin Hosner or Davide Silvagni, respectively. This was very time consuming in both cases, so the amount of discharges for which these validation techniques could be conducted is limited. A more in-depth discussion on the different validation techniques can be found in their sections in this chapter. The validation technique based on the temperature profile of the edge Thomson scattering diagnostic was done for discharge #34275 to confirm the two-point model validation of this shot. Discharges 34027 – 34063 where also analyzed with the Thomson scattering technique. The two-point model validation was conducted for discharges #33052 – #33054 and #34275. For the strike point validation two upper single null discharges were used: #34304 and #34238. Additionally the lower single null discharge #32212 was used. The discharges used in each validation technique can also be seen in table 1 in Appendix A.

5.2 Thomson Scattering Validation

One possibility of validation is to use the property of the plasma, that in H-mode, the electron temperature is typically between 80 and 120 eV at the

separatrix, limited by the dissipation of energy in the SOL due to transport processes [26, 27]. This information can be used to predict the location of the separatrix in kinetic temperature profiles measured by diagnostics like the vertical Thomson scattering or electron cyclotron emission diagnostics. This predicted location of the separatrix can then be compared to reconstructed separartix contours to validate them.

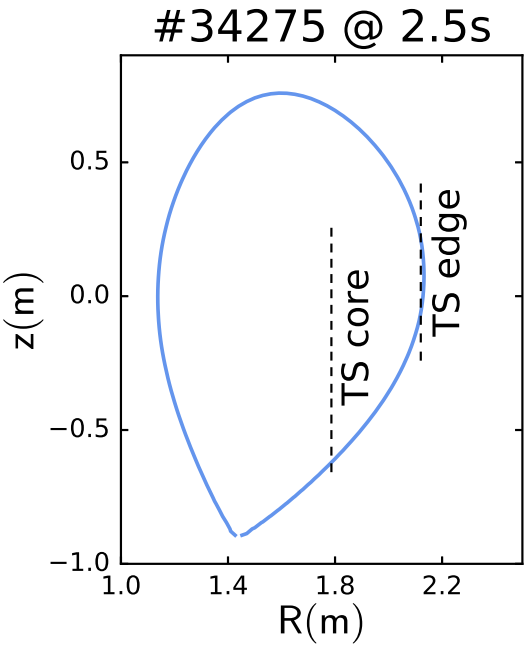

FIGURE 5.1: Separatrix contour relative to scattering volumes of TS diagnostic

The first candidate for a temperature diagnostic was the vertical Thomson scattering diagnostic [16]. Thomson scattering uses lasers to scatter light off of electrons in plasmas. The velocity distribution of the electrons causes a Doppler shift in the measured wavelength distribution of the scattered light. This can then be used to measure the electron temperature [28]. Additionally the intensity of the scattered light is used to determine the electron density.

At ASDEX Upgrade the vertical Thomson scattering diagnostic consists of two systems, the core TS system and the edge TS system. The location of the scattering volumes of the two diagnostics compared to a typical separatrix contour can be seen in Fig. 5.1. The core TS system is intersected by the separatrix at one point of the lower part of the low-field side. The separatrix intersects the edge TS system up to two times. This depends on how far out the furthest outer radial point of the separatrix contour (R_{aus}) is. Typically the TS system will intersect with the separatrix three times on different parts of the contour, making it a valuable validation tool.

Unfortunately, the vertical TS diagnostic has a low temporal resolution. Each of the lasers triggers with a frequency of 20 Hz. The edge TS diagnostic uses a total of 6 lasers, while the core TS diagnostic uses 4 [16]. This means

that contour changes on a very short time scale cannot be validated using the TS diagnostic.

Another major issue with the Thomson diagnostic is a large, unexplained radial shift. When comparing temperature or density profiles of the TS diagnostic at ASDEX Upgrade to the same profiles of other diagnostics, such as those of the electron cyclotron emission, lithium beam or reflectometry diagnostics, the TS profile has to be radially shifted to be aligned with the other profiles. This radial shift is typically 2.5 – 5 cm inwards for the core TS profile and 6 mm outwards for profiles of the edge TS diagnostic.

To quantify this effect a total of 120 time windows of relatively constant stored magnetohydrodynamic plasma energy (W_{MHD}) of 35 discharges were analyzed. In each of these time windows the Thomson temperature profile mapped with CLISTE was compared to the integrated data analysis profile, which is generally mapped using the CLISTE equilibrium. The Thomson profile was then radially shifted until the IDA and Thomson temperature profiles matched. An example of this technique can be seen in Fig. 5.2. Here the blue dots are the temperature measurements of the core TS diagnostic and the blue crosses the measurements of the edge TS diagnostic. Both of the TS temperature profiles are mapped using the CLISTE equilibrium to the normalized radius ρ_{pol}. The black lines are the IDA temperature profiles in the time window. On the left side of Fig. 5.2 all profiles are shown without being shifted. On the right side a shift of 3.8 cm inwards is applied to the core TS profile and an outwards shift of 6 mm to the edge TS profile. This is done by adding or subtracting the radial shift to the radial coordinate of the laser in use at the time of the temperature measurement, as is typically done when analyzing data in analysis programs like augped [29]. The alignment of the Thomson profiles is much better on the right side of Fig. 5.2, but the temperature gradient is steeper than that of IDA which is mainly determined by ECE measurements.

The results of this study were that typically the core TS profile had to be shifted inwards by 3 cm. This can vary considerably, however. The lowest necessary shift in these time windows was 1 cm (#34265 t=2.0 – 3 s) and the highest was 7 cm (#33616 t=1.8 – 3 s). In the majority of cases it around 3 cm, however. The radial shift of the core TS profile was prone to changing considerably in magnitude during different phases of discharges as well as in between discharges. In an effort to explain the causes of this shift and be able to use the core TS diagnostic as a validation tool an extensive study was conducted to quantify the different uncertainties going into the radial shift. This study will be discussed in section 5.2.1. The result was, however, that the shift could not be properly explained and because of this the core TS diagnostic was not used for validation purposes.

The edge TS profile was also subject to an unexplained radial shift and in the study of the radial shifts within the different time windows had to be shifted outwards between 6 mm and 8 mm, with 6 mm being the far more common case. It was also discovered that in general the shift of the edge TS

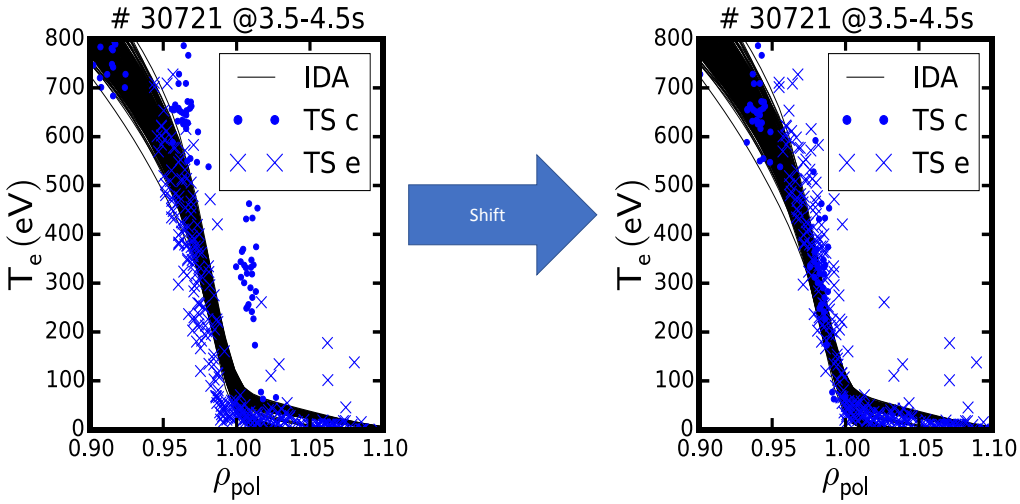

FIGURE 5.2: Typical TS shift example. The core TS diagnostic was shifted by 3.8 cm inwards and the edge TS 6 mm outwards on the right side.

diagnostic was constant throughout the entire discharge. All of the discharges used in the edge TS validation were in the group with the typical shift of 6 mm. For these reasons the edge TS diagnostic was used as a validation tool with a constant 6 mm outwards shift to the location of the scattering volumes. The methodology of this validation technique will be discussed in section 5.2.2.

5.2.1 Uncertainty in TS Core Diagnostic

As discussed in section 5.2 the core TS diagnostic is prone to a large, unexplained radial shift when compared to other diagnostics. This shift had to be explained to use measurements from the core TS diagnostic for validation purposes. In this section the different estimations of the possible partial uncertainties as well as the total uncertainty estimation based on them will be discussed.

5.2.1.1 Equilibrium

To better be able to compare the profiles of the TS diagnostics to profiles of other diagnostics, the profiles are usually mapped onto coordinates on the basis of flux surfaces. This means that an uncertainty in the equilibrium could lead to a shifted TS profile when compared to other profiles like the ECE diagnostic which uses channels with locations based on the total magnetic field.

5.2.1.1.1 Effects of Input parameters For this reason the uncertainty of the separatrix contour around the core TS diagnostic had to be estimated. The strongest influence on this part of the separatrix contour is the lower

PSL due to its immediate proximity. For this reason a sensitivity study was conducted (section 4.3.2). The PSL sensitivity study showed, that the typical uncertainty of 6 mm at the intersection point of the core TS diagnostic with the separatrix contour, was not enough to explain the 3 cm shift typical for the core TS diagnostic. The shift caused by the absence of a current fit in the PSL also shifts the position of the separatrix inwards at the core TS diagnostic, which is the wrong direction to explain the shift.

Using some of the other effects discussed in chapter 4 can alleviate some of the radial shift in both the edge and core TS diagnostics. For example the larger allowed variability discussed in section 4.3.1 often reduces the amount of radial shift of the edge TS diagnostic. This effect does not impact all discharges the same, however. The same can be said for using the scrape-off layer modeling discussed in section 4.4. In some cases using equilibria with enabled scrape-off layer current fit to map the core TS channels will reduce the amount of radial shift considerably, while in other cases this effect does not impact the location at all. The same can be said for the fast ion modeling discussed in section 4.5. This implies that none of the previously examined input parameters are the sole cause of the radial shift.

5.2.1.1.2 Contour Shape Another reason to doubt the equilibrium as the main cause of the radial shift of the core TS channels is the fact that the edge TS channels have to be shifted outwards in order to align their temperature and density profiles with those of other diagnostics, while the core TS channels have to be shifted inwards. This means that if the shift of the TS diagnostics was equilibrium based, the whole contour shape at the lower half of the LFS would have to be changed. The contour would have to be shifted inwards at the midplane while at the same time being shifted outwards at the core TS channels.

In order to test this explanation a study was conducted by Rainer Fischer where the contour of the separatrix was artificially altered as much as possible by changing input parameters while still having a convergent solution for the equilibrium. This led to the conclusion that even with very strong artificial changes only, a very small change of shape of the separatrix could be observed [10].

5.2.1.2 Scattering Volume

Another possible reason for the radial shift in the core TS channels could be that because TS measured the electron temperature by scattering light off of electrons, the location of the measurement is weighted towards the part of the scattering volume with a higher electron density. So if the scattering volume encompasses a volume of the plasma with a high density gradient, a majority of the scattered light will come from the part of the scattering volume with the higher electron density.

At ASDEX Upgrade the scattering volumes observed by the polychromators of the TS diagnostics is defined by the thickness of the laser and the height of the window that is observed by the polychromators. The lasers used in the ASDEX Upgrade TS system have a thickness of 2.7 mm and the scattering volumes of the core and edge TS diagnostics have a height of 25 mm [16]. This means that the radial uncertainty caused by the laser thickness can be neglected in this estimation because it is much smaller than the 3 cm of uncertainty typically observed in the core TS diagnostic. The typical location of the TS scattering volumes relative to the separatrix can be seen in in Fig. 5.1.

The middle of the scattering volumes are used for the location of the measured data. This means that in the worst case, the total data attributed to the middle of the scattering volume would be collected at one edge of the volume. So the uncertainty in z-direction in the worst case scenario would be 12.5 mm.

The separatrix was used to estimate the radial displacement because this effect would only have a strong influence in areas with a high density gradient. The separatrix typically has an angle of incidence of about 45° onto the TS scattering volumes. This means that the maximum radial uncertainty can be estimated to 13 mm, which is not enough to explain the 3 cm typical uncertainty.

Another argument speaking against this explanation of the shift is that a shift caused by the finite scattering volume would only be possible in cases where the affected scattering volume is within a part of the plasma with a high density gradient. This would make the TS shift highly case dependent. But the separatrix moves around in each discharge and is positioned differently in different discharges. While it is possible that this effect exists it is likely not the cause of the shift observed in almost every shot.

5.2.1.3 Uncertainty in the Position of the Scattering Volumes

Another possible cause of the radial shift is an uncertainty in the knowledge of the location of the diagnostic within the vessel. This is also unlikely because the location of the vacuum windows used by the diagnostic was measured by the FARO system which is accurate on the order of mm.

5.2.1.4 Results

Even when all of the examined effects are combined the resulting uncertainty is not enough to explain the radial shift typically observed in the core TS temperature and density profiles. Because of this unexplained and unpredictable uncertainty the core TS diagnostic is not a viable candidate for use as a validation technique.

5.2.2 Edge Thomson Scattering Validation

The edge TS diagnostic was used to validate the separatrix contour around the low-field-side midplane. As justified in section 5.2 a constant radial shift

of 6 mm outwards was applied to the location of all TS lasers.

5.2.2.1 Approach

In order to use the TS diagnostic as a validation tool, first suitable cases had to be found. This is done by looking at the location of different separatrix contours relative to the edge Thomson lasers during different discharges. An example of these locations can be seen in Fig. 5.3.

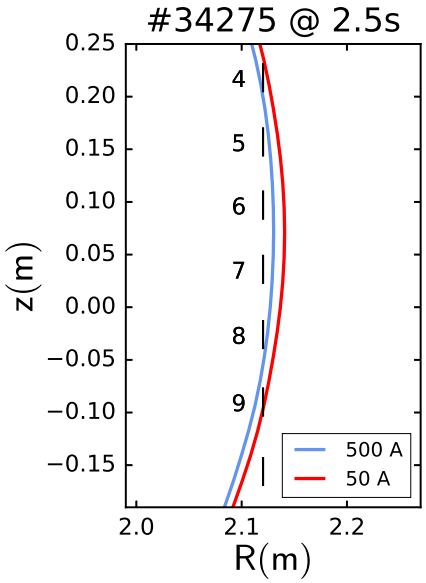

FIGURE 5.3: Intersection points of the different separatrices with the TS scattering channels in #34275

Here the discharge discussed in section 4.3.1 can be seen but at a different time point. There are two different separatrix contours, one based on an equilibrium with an allowed variability of 50 A to the current measured in the V-coils and one with an allowed variability of 500 A. Also shown are the scattering volumes of the TS diagnostic at that time. These shift in radial position as different lasers are cycled by 8 mm in the core TS diagnostic and 19 mm in the edge TS diagnostic. In this figure, we can see that on the lower half of the LFS contour the green line intersects with the TS channel 9. The blue separatrix contour is shifted further inwards and does not intersect with this scattering volume. On the upper part of the LFS contour the blue separatrix intersects scattering volume 4 on the lower border, while the green separatrix intersects the same scattering volume on the upper border. This means that the green equilibrium predicts TS channels 9 and 4 to be largely within the confined part of the plasma, i.e. inside of the separatrix. This would mean one would expect a measurement of around 100 eV in this TS channel if we were to believe the green equilibrium. The blue equilibrium predicts the same TS channel to be outside of the separatrix, in the SOL. This would mean that the TS channel should measure a temperature of much lower than 100 eV. This

information is then compared to the temperature measurement in Thomson channels 4 and 9 at the same time, which in this case is 56 eV and 43 eV respectively. This means, that at this time point both the Thomson channels corroborate the prediction of the blue separatrix. In this fashion all time points of the TS diagnostic can be analyzed during a discharge, allowing for a much more sound statement over the reliability of the individual reconstructions. In this discharge the equilibrium with tighter constraints consistently predicts the TS channel 9 to be between the separatrix and the plasma core while the equilibrium based on the looser constraints consistently predicts the scattering volume to be in the scrape-off-layer, thus predicting a measured temperature of less than $80-120$ eV. Unfortunately the angle of incidence between channel 4 and the separatrix is much lower. This means a small radial change in the separatrix can shift the scattering volume from being entirely inside the confined part of the plasma to the scrape-off layer. In this case this effect leads to both separatrices predicting channel 4 to be inside and outside of the confined plasma regime. The temperature measured in channel 4 reflects this in a very high temperature spread and so corroborates the predictions of the separatrix contours of both equilibria. This makes it illegible for validation in the case of #34275.

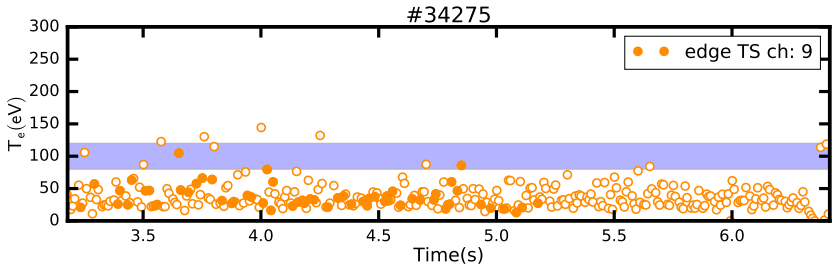

FIGURE 5.4: Time trace of the temperature measured in edge TS channel 9 in #34275

In Fig. 5.4 the temperature measured by TS channel 9 is shown during the discharge. The empty circles are measurements close to edge localized modes (ELMs), which are strong disturbances of the plasma in a short period of time. Close to ELMs the 100 eV criterion is not necessarily fulfilled. The temperature mostly stays below the temperature region of 80 – 120 eV, marked in blue, that would be expected for the separatrix. This means that the TS-based validation technique indicates that the TS channel is in the SOL. This supports the reconstructed separatrix based on the allowed 500 A variability in the V-coils.

5.2.2.2 Issues

This validation technique has some issues, however. One problem is that the exact temperature at the separatrix is not known. This means that the mea-

sured temperature in the TS channel has to be outside of the wide range of $80 - 120\,\mathrm{eV}$ for a clear validation.

Another problem is the radial shift of the edge TS diagnostic discussed in section 5.2. The data used for the measurement of the shift is necessarily based on equilibria. Even though in the method discussed in section 5.2 the same equilibrium was used for mapping the profiles of both the TS and IDA, the uncertainties of that equilibrium could still have influences on the 6 mm constant shift that were ultimately used in this validation.

The final problem is that the bias of the temperature measurement towards the area within the scattering volume with higher electron density, discussed in section 5.2 is not quantified and so its influence not thoroughly understood.

For all of these reasons only very clear examples can be used in this validation technique. This means a large difference in position of the separatrix contour is needed to make a clear statement over the results. The amount of required difference is often larger than the typical difference of many of the phenomena analyzed in chapter 4. Additionally the different separatrices need to be positioned on separate sides of the scattering volume to be able to use this technique. These issues greatly reduce the number of eligible discharges and influences on the separatrix that can be validated with this technique.

5.2.3 Two-Point Model Validation

In this section another validation technique will be discussed. In this technique the temperature at the separatrix is predicted with the two-point transport model. A fit is found to describe the radial decay of a temperature profile. This can be either the temperature profile provided by the Thomson scattering or integrated data analysis (IDA) diagnostic. The fit is used to estimate the radial decay length of the electron Temperature. To ensure the physical accuracy of the fit it is chosen using the two-point model [27]. The resulting decay length is used to estimate the electron temperature of the separatrix, which is then used in the fitted temperature profile to determine the separatrix location. This evaluation was done by Martin Hosner [30]. The result of this analysis is a prediction of the temporal evolution of the outer most radius of the separatrix (R_{aus}). This prediction can then be compared to the predictions of individual equilibria to corroborate the different settings on which those equilibria are based.

As an example of this technique the case of discharge #34275, which was discussed in section 4.3.1 and was validated in section 5.2.2 will be analyzed. In this analysis different settings for the allowed variability in the current of the V-coils, marked in green in Fig. 3.3 were used to reconstruct two separate equilibria. The predictions of the outer most point of the separatrix contour (R_{aus}) using different settings for this allowed variability vary quite significantly and this discrepancy grows continuously during the later stages of the discharge. The predictions of the two different IDE equilibria as well as some predictions by the two-point model are shown in Fig. 5.5. The magenta line describes the

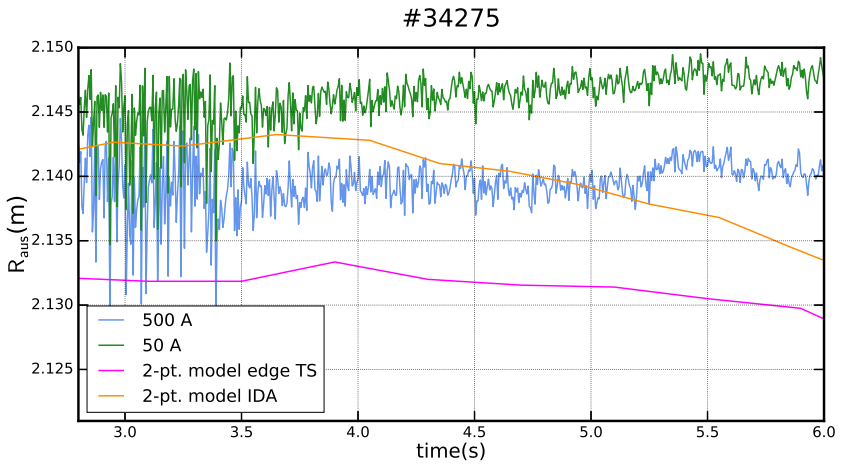

FIGURE 5.5: Predictions of R_{aus} in discharge #34275 by different IDE equilbria and two-point model based on TS or IDA data

two-point model prediction based on data from the edge Thomson scattering diagnostic data. This prediction is about 8 mm lower than the prediction of the equilibrium based on 500 A of allowed variability. The typically predicted electron temperature at the separatrix by the two-point model based on edge Thomson scattering measurements is about 120 eV in this discharge, which is on the upper boundary of the expected electron temperature at the separatrix. This leads to a separatrix position that is further inwards than would normally be expected. The reason for this could be that the electron temperature profiles of the edge Thomson scattering diagnostic used as a basis for this evaluation have a very high temperature gradient, as well as some high temperature measurements that are often assumed not to be reliable. Together this could lead to an overestimation of the separatrix temperature, which in turn would lead to a separatrix position that is shifted inwards by an unphysical amount. The orange line shows the R_{aus} estimation of the two-point model validation technique based on IDA profiles. The estimated location starts out between the two estimations of the different IDE equilibria but the position is shifted further inwards in the later stages of the discharge. This positional change is most likely due to the fact that in the later stages of the discharge a nitrogen puffing event takes place, which would normally be expected to lower the electron temperature, but this effect is not accounted for in the two-point model [30]. This could lead a loss of reliability when choosing the exact fit for the radial temperature profile, which in turn would again lead to an overestimation of the separatrix temperature and in turn a separatrix closer to the core of the plasma than expected. This means in this case the two-point model validation cannot be used to make a clear statement on the reliability of the different equilibria.

5.2.4 Combination of Techniques

The validation at the midplane was conducted using the temperature profile of the edge Thomson scattering diagnostic and an estimation of the temperature of the separatrix at the midplane based on the two-point model.

In chapters 5.2.3 and 5.2.2 the examples of the validation shown were for the same discharge. The edge TS validation works around the midplane, while the two-point model validation validates at R_{aus}, which is typically within 10 cm of the midplane. This means that the results of the two different validation techniques can now be combined in order to either corroborate or to invalidate their results. It is important to realize, however, that both of these validation techniques are based on the edge TS temperature profile. This means they can both be subject to the same uncertainties.

Unfortunately due to the ambiguous results of the two-point validation technique, no clear statement can be made in the example of #34275, although the edge TS based validation favors the equilibrium based on the 500 A variability in the V-coils. This led to the decision to use this setting in the baseline equilibria (see section 4.6) against which all other equilibria were compared in chapter 4. In other examples combining the different techniques could lead to a more substantiated validation of the separatrix around the low-field side midplane.

5.3 Strike Point Validation

Another important part of the separatrix contour is the part of the contour between the X-point and the divertors. One way of validating the separatrix here is through strike point validation. The strike point of a fusion plasma is the point at which the contour of the separatrix intersects the divertor of the tokamak. An example of this part of the contour can be seen in Fig. 5.6.

In order to be able to validate the strike points, measurements taken by the thermography diagnostic are used to determine the actual strike point of the plasma. The power deposition onto the divertor plates is fitted to find the point of highest power deposition. This is done by fitting a function made up of a combination of a Gaussian and an exponential decay from the point of the expected beginning of the scrape-off layer as shown in Fig. 5.7. The maximum of the resulting function is then the strike point, the point where the separatrix intersects with the divertor plate [31, 32]. The strike point is validated by plotting the time-trace of the strike point based on the thermography diagnostic against the predictions of different equilibria.

As mentioned in chapter 4.1 a strike point validation was conducted on the lower divertor for an L-mode discharge (#32212), the results of which can be seen in Fig. 5.8. The difference between equilibria of L-mode discharges is very slight between IDE and CLISTE. This holds true for the location of the strike line as well. The difference in location of the predicted strike point is typically about 2 mm in discharge #32212. Both of the equilibrium strike

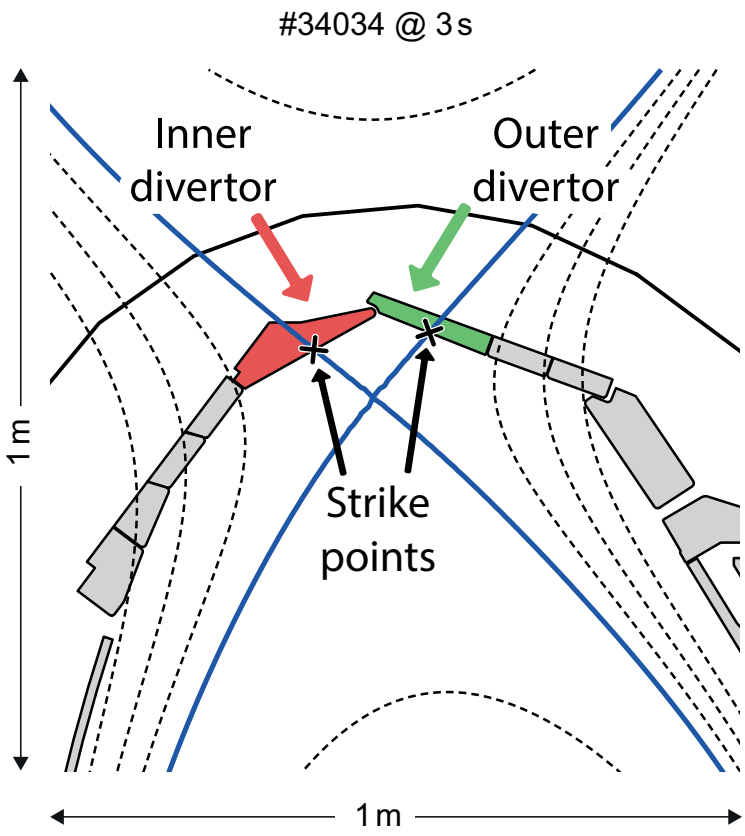

FIGURE 5.6: Example of location of the strike points on the upper divertors

point predictions fall into the uncertainty of the thermography prediction,for a majority of time points, so in this case no clear statement over the reliability of the different equilibria can be made.

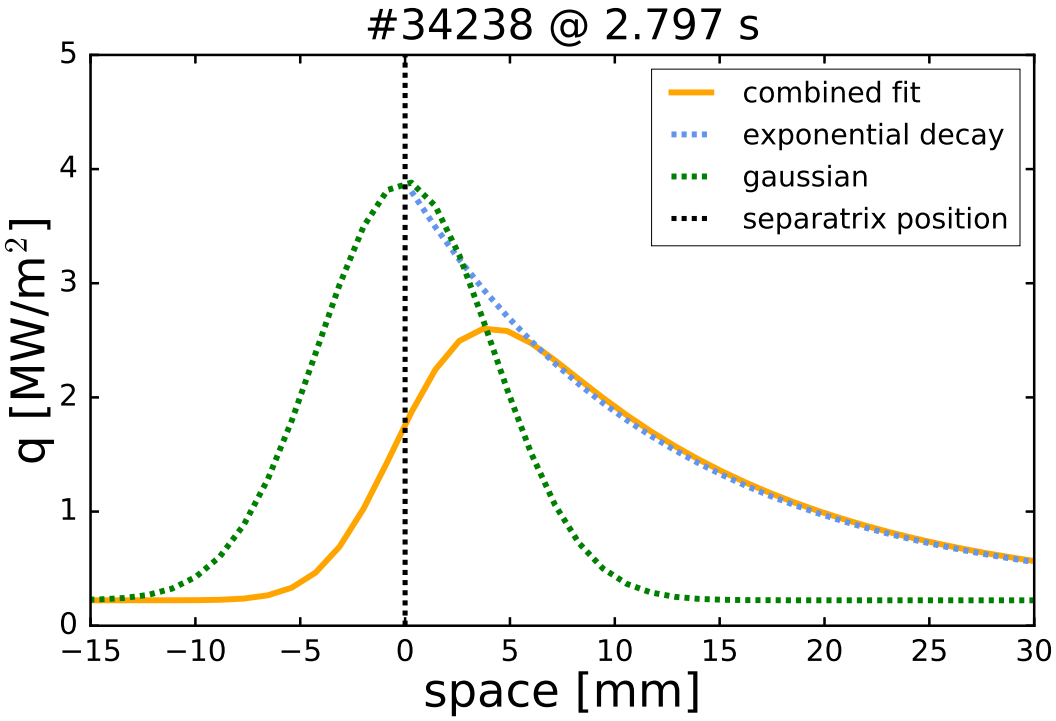

FIGURE 5.7: Example of fit used to estimate the location of the strike point

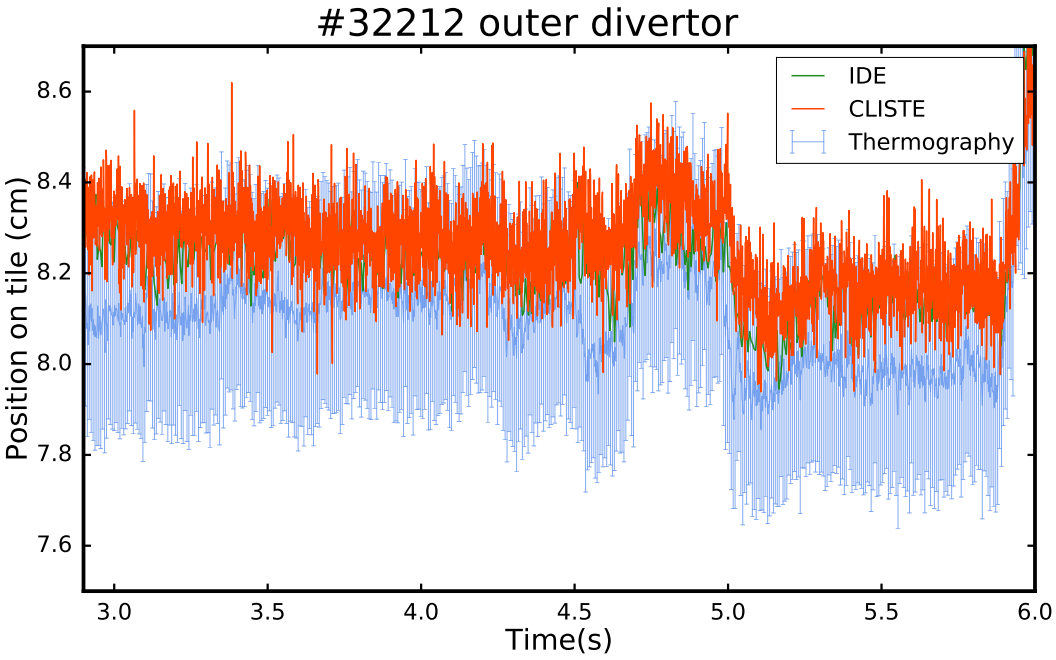

FIGURE 5.8: Fitted strike point compared to predictions by IDE and CLISTE for #32212 in the outer, lower divertor

In figs. 5.9 and 5.10 the resulting validation can be seen for two shots for the outer and inner upper divertor.

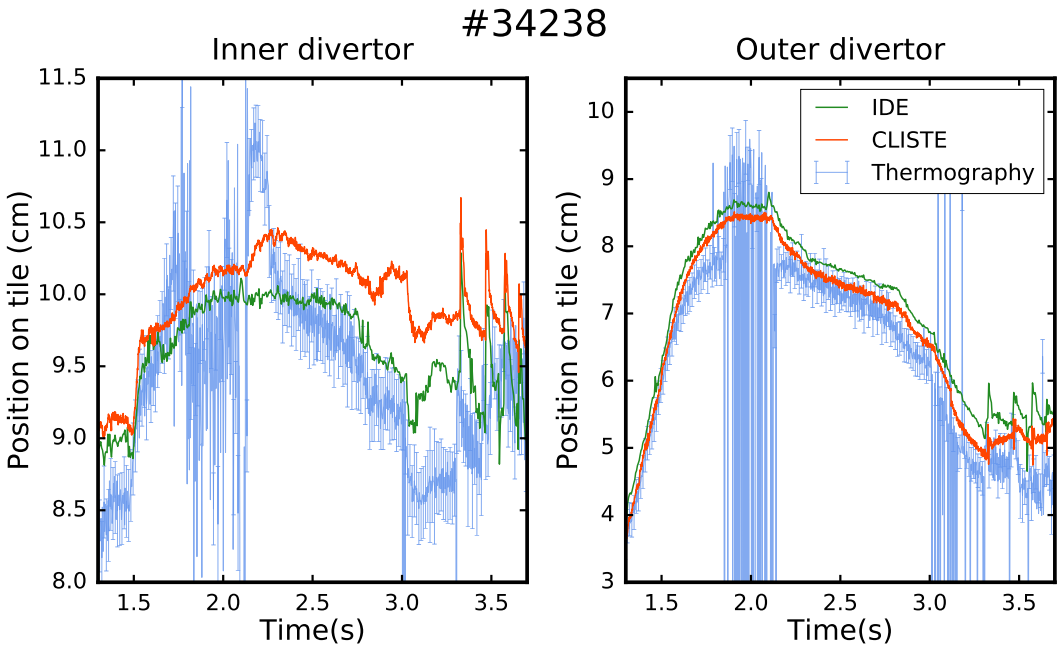

FIGURE 5.9: Fitted strike point compared to predictions by IDE and CLISTE for #34238 in the upper divertors

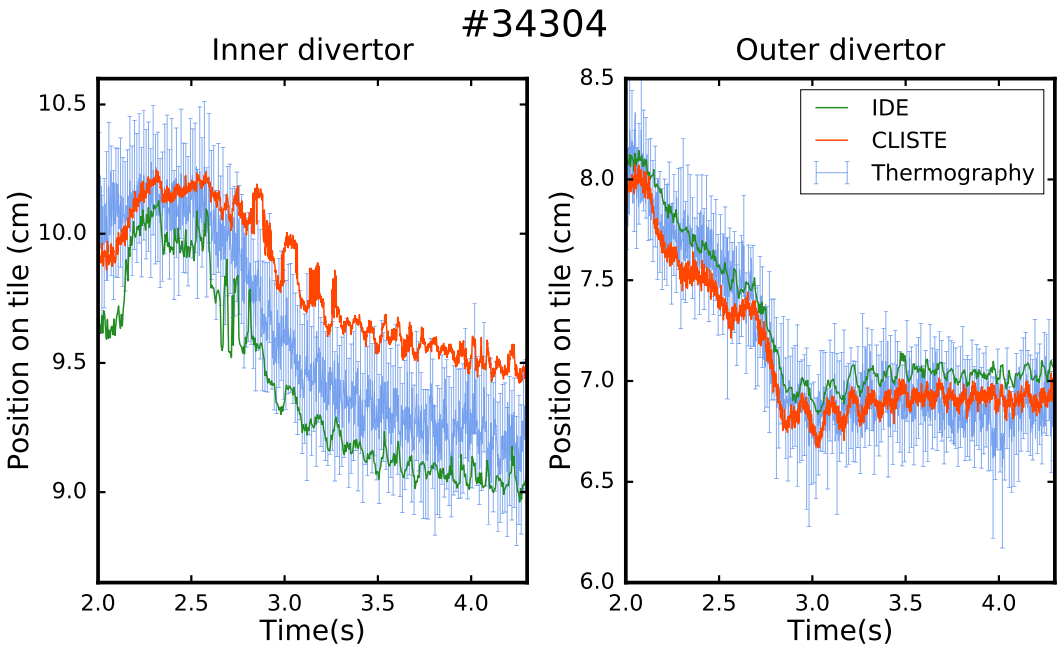

FIGURE 5.10: Fitted strike point compared to predictions by IDE and CLISTE for #34304 in the upper divertors

In discharge #34238 the thermography measurements corroborates the IDE separatrix on the inner divertor, while it supports the CLISTE prediction on the outer divertor. In discharge #34304 both of the predicted strike point time traces are within the uncertainty boundaries of the thermography prediction, so in this case, again the validation did not allow for a distinction between the reliability of the different equilibria.

Chapter 6

Summary and Conclusions

In this work the uncertainties in the separatrix contour were estimated. A sensitivity study was conducted to quantify the effects of different influences on the separatrix contour. This shed light on some large and often not well understood uncertainties. Different validation techniques were used to analyze the reliability of the different reconstructed separatrices on different parts of the contour. In many of the sensitivity studies it became apparent that seemingly small uncertainties, such as the 1% current uncertainty in the validation process of the magnetic probe arrays can lead to very significant differences in the reconstructed separatrix contour. At the same time individual quantities can have a much stronger influence than competing quantities. An example of this is that the shape of the difference profile caused by disabling the current fit in all poloidal field coils is dominated by the shape of the disabled current fit in the lower PSL. This means it is important to first analyze a complete set of input parameter and later the individual parameters to pinpoint the parameter, where reducing the uncertainty yields the most benefit to the reconstructed equilibrium. In this case, the reduction of the uncertainty in the measured PSL current could help reduce the uncertainty caused by the measured current in all coils.

The separatrix contour, even though it is very important for fusion research might be subject to large uncertainties. Its uncertainty depends on many factors and can be on the scale of cm at ASDEX Upgrade. One should be aware of these uncertainties and not use the separatrix contour as a given quality without uncertainties.

The influence of uncertainties in magnetic measurements on the separatrix contour can be detrimental to the quality of the resulting equilibrium. Uncertainties in the measurements of the poloidal magnetic field lead to an difference of typically 5 mm along the lower half of the separatrix contour. This means that in order to improve equilibrium reliability a big step could be taken by taking a closer look at the calibration uncertainties in the magnetic measurements themselves and trying to reduce them as much as possible. Another important step would be to provide complementary magnetic measurements to be able to compare the different data and gain a clearer understanding over

their uncertainties.

Uncertainties in current measurements in the poloidal field coils also have a large influence on the uncertainties of the separatrix contour. Increasing the allowed variability of the current fit in the V-coils led to a typical difference of 5 mm inwards at the midplane. The contour of the separatrix based on the higher allowed variability was later validated by two different techniques for the analyzed discharge. This means that at least in this case the modeled current appears more plausible. If this is true in general the current measurements in the V-coils are subject to unknown uncertainties. Reducing these uncertainties would certainly improve the equilibrium.

The PSL also has a large influence on the separatrix contour. The uncertainties in the current of the lower PSL in particular strongly influence the uncertainties of the currents in the lower half of the LFS. This can be seen when comparing the difference profile of the current in all coils with that of the lower PSL. The shape of the difference profile of the PSL current is virtually identical with that of the lower half of the LFS difference profile. So understanding the PSL current uncertainties is incredibly important to the total difference in the vacuum field. Sadly due to the unexplained shift in the core TS diagnostic a validation of this part of the separatrix contour and through it an estimation of the optimal amount of allowed variability in the PSL current was not possible.

The influence of the modeling of the scrape off layer current fit was also analyzed. This quantity influences the separatrix contour predominantly at the X-point, with a large outward shift of the X-point of up to 4.4 cm, but more typically 2 cm.

Fast-ion modeling is also very important to the quality of the separatrix contour. The influence of fast-ions on the separatrix contour is based on the amount of NBI power in a given discharge as well as the plasma current. A higher NBI power leads to a larger difference of the separatrix contours at the midplane. This effect was up to 12 mm in the discharges analyzed. The uncertainty on the upper and lower part of the LFS contour as well at the X-point contour are strongly influenced by the plasma current. A discharge with roughly the same amount of NBI heating and with an I_p of 0.6 MA instead of 0.8 MA can have an uncertainty that is up to 1 cm higher in these regions. This means that not using fast-ion modeling has been observed yielding an uncertainty of up to 22 mm. So the uncertainties of the fast-ion modeling can influence the separatrix contour strongly.

The influences going into the uncertainties of the separatrix contour are often hard to pinpoint because of the complex nature of equilibrium reconstruction. This could be seen in the sensitivity study of the magnetic data preprocessing. Here the naive prediction of creating a more similar equilibrium to CLISTE in IDE when using the same magnetic preprocessing as CLISTE did not come true, because of the different information sources used by the two equilibrium solvers.

The validation techniques used in this thesis were in their early stages

and only applicable to a select set of scenarios. But even so they provided an important point of reference to make use of the data provided by the sensitivity studies. The combination of the validation techniques at the midplane allowed for an educated choice of the allowed variability in the V-coils in all of the standard equilibria used as points of reference in the sensitivity studies. This hopefully reduced the uncertainties of all of these studies.

Even with their limitations the validation techniques were very beneficial when trying to interpret the results of the sensitivity studies. In the future they could possibly be supplemented with other techniques based on the density profiles. It might also be possible to automate some parts of the processes, facilitating the analysis of more scenarios.

The uncertainty caused by the calibration of the magnetic probe arrays might be resolved when measurements of the three additional arrays become available in future campaigns. This would certainly improve the reliability of both the IDE and CLISTE equilibria.

Appendix A

In this Appendix, the discharges used in this thesis are listed. Additionally some important plasma parameters for each discharge are given, as well as the analyses each of the discharges was used in.

#	$B_t(T)$	$I_p(MA)$	q_{95}	$n_e(m^{-3})$	t	used in analysis
30701	-2.5	1.0	4.2	8.1×10^{19}	2.9 – 3.4 s	V PSL
30721	-2.5	1.0	4.3	7.9×10^{19}	3.1 – 5.5 s	V PSL
32032	-2.5	0.8	5.0	8.3×10^{19}	4.1 – 8.4 s	V PA PSL
32148	-2.5	0.8	5.3	5.6×10^{19}	2.3 – 8.1 s	V PA FI PSL
32149	-2.5	0.8	5.2	6.0×10^{19}	2.5 – 5.5 s	V PA FI PSL
32212	-2.5	0.8	4.9	1.87×10^{19}	2.0 – 5.9 s	PSL TH
33052	-2.5	0.8	4.8	6.6×10^{19}	3.4 – 6.0 s	V PSL 2P
33053	-2.5	0.8	4.8	7.8×10^{19}	3.2 – 6.2 s	V PSL 2P
33054	-2.5	0.8	4.8	8.0×10^{19}	3.2 – 6.3 s	V PSL 2P
33134	-2.5	0.8	5.2	5.2×10^{19}	3.4 – 7.0 s	V PA FI CF SOL PSL
33173	-2.5	1.0	4.1	9.1×10^{19}	1.5 – 7.5 s	V FI CF SOL PSL
33178	-2.5	0.8	5.3	6.1×10^{19}	2.2 – 5.0 s	V PA FI CF SOL PSL
33379	-2.5	0.6	7.1	4.8×10^{19}	3.3 – 8.0 s	V PA FI CF SOL PSL
33421	-2.7	1.0	4.6	4.0×10^{19}	2.5 – 7.0 s	V PA FI CF SOL PSL
33500	-2.5	0.8	4.8	7.8×10^{19}	2.5 – 5.0 s	V PA FI CF SOL PSL
33616	-2.5	0.8	5.2	6.5×10^{19}	1.8 – 6.0 s	PA CF SOL PSL
33692	-2.5	1.0	4.4	5.2×10^{19}	2.0 – 3.7 s	PA FI CF SOL PSL
33856	-2.5	0.8	5.2	7.0×10^{19}	1.8 – 6.4 s	PA FI PSL
33857	-2.5	0.8	5.1	7.0×10^{19}	1.7 – 6.4 s	PA FI PSL
33864	-2.6	0.8	5.2	5.7×10^{19}	2.2 – 7.6 s	PA FI PSL

34027	−2.5	0.8	5.3	6.7×10^{19}	1.3 – 8.8 s	PA FI PSL TS
34041	−2.5	0.8	5.4	7.3×10^{19}	1.4 – 8.4 s	PA FI PSL TS
34042	−2.5	0.8	5.4	6.8×10^{19}	1.3 – 8.6 s	PA FI PSL TS
34047	−2.5	0.8	5.3	6.7×10^{19}	1.3 – 8.4 s	PA FI PSL TS
34048	−2.5	0.8	5.3	7.3×10^{19}	1.3 – 8.4 s	PA FI PSL TS
34049	−2.5	0.8	5.3	7.0×10^{19}	1.3 – 8.5 s	PA FI PSL TS
34050	−2.5	0.8	5.3	7.0×10^{19}	1.3 – 8.5 s	PA FI PSL TS
34051	−2.5	0.8	5.3	7.0×10^{19}	1.3 – 8.6 s	PA FI PSL TS
34062	−2.5	0.8	5.3	8.0×10^{19}	1.4 – 8.6 s	PA FI PSL TS
34063	−2.5	0.8	5.3	7.8×10^{19}	1.4 – 8.5 s	PA FI PSL TS
34218	−2.5	0.8	5.3	5.3×10^{19}	3.4 – 6.9 s	PA FI PSL
34219	−2.5	0.8	5.3	5.6×10^{19}	1.6 – 5.1 s	PA FI PSL
34226	−2.5	0.6	7.9	4.3×10^{19}	1.3 – 8.9 s	PA FI PSL
34238	−2.5	1.0	3.9	11.0×10^{19}	3.3 – 3.7 s	SOL PSL TH
34265	−2.5	0.6	6.6	5.6×10^{19}	1.2 – 9.0 s	PA FI PSL
34275	−2.5	0.8	5.0	8.4×10^{19}	2.5 – 6.3 s	V PSL TS 2P
34304	−2.5	1.0	3.9	5.3×10^{19}	2.9 – 4.3 s	PSL TH
34406	−2.5	0.8	5.3	5.3×10^{19}	3.4 – 6.7 s	PA FI PSL
34483	−2.5	1.0	4.4	9.6×10^{19}	3.0 – 6.3 s	V PSL
34532	−2.5	0.8	5.1	7.5×10^{19}	1.8 – 7.3 s	PA FI PSL
34549	−2.5	0.6	7.0	3.7×10^{19}	2.8 – 4.3 s	FI PSL
34658	−2.6	1.0	4.4	5.1×10^{19}	2.3 – 6.5 s	PA FI PSL
34660	−2.6	1.0	4.4	4.0×10^{19}	2.9 – 6.5 s	PA FI PSL
34664	−2.5	1.0	4.3	4.6×10^{19}	2.8 – 6.2 s	PA FI PSL
34671	−2.5	1.0	4.1	4.8×10^{19}	2.8 – 6.4 s	FI PSL

Table 1: Discharges with plasma parameters and studies used. Abbreviations explained in text

The studies in which the individual discharges were used can be seen in the column on the right of table 1. Here the different abbreviations indicate the discharge was used in:

- sensitivity studies of:
  - V: V-coil current fit (section 4.3.1)
  - PA: probe arrays (section 4.2.1
  - FI: fast-ion modeling (section 4.5)
  - CF: current fit in all coils (section 4.3.3)
  - SOL: scrape off layer current fit (section 4.4)
  - PSL: PSL current fit (section 4.3.2)
- validation techniques using:
  - TS: edge Thomson scattering (section 5.2.2)
  - 2P: two-point model (section 5.2.3)
  - TH: thermography diagnostic (section 5.3) of the strike point.

Acknowledgments

First and foremost I would like to thank my supervisor, Dr. Rainer Fischer for always being available for questions and guidance, while at the same time giving me the possibility to find my own solutions to problems and listening their explanations patiently before helping me find much more practical solutions. He made my thesis a very enjoyable and educational experience and always made time to help me.

I also want to thank Prof. Dr. Ulrich Stroth for giving me a chance to work at IPP as a working and later diploma student. Through this I had the opportunity to work in a field that has been my major fascination, since I first learned about it in school.

My special thanks also go out to Dr. Elisabeth Wolfrum for introducing me to fusion research during my time as a working student and for taking hours of time out of her busy schedule to let me benefit from her encyclopedic knowledge of fusion physics and research.

Thank you very much to Davide Silvagni for the endless hours spent on providing me with data to use in the strike point validation, even if it meant staying much later on Friday evening than he would have expected.

I also want to thank Martin Hosner for taking the time to provide me with data for the two-point model validation and doing this during very stressful parts of his own thesis and late in the evenings.

Thank you very much to Daniel Kuenz for helping me improve the quality of the figures for my thesis even at ungodly times of the night.

Thank you also to all of my office cohorts: Josh McMahon, Klara Höfler, Alexander Bauer, Thomas Reichsbauer, Lennart Bock, Stephan Glöggler, Severin Denk and Theobaldo Luda di Cortemiglia for making the entire thesis a much more entertaining experience, for making the more frustrating parts of the thesis much more enjoyable and for listening to my stupid ideas and incoherent ramblings for hours on end.

Thank you to Dr. Felician Mink for very patiently explaining the basics of fusion research and scientific programming to me.

Thank you to Dr. Alexander Bock for the always available IT support and for the continued but ultimately futile effort to make me program like a normal person and for taking the time to think through the inane ravings that make up my code.

A very special thank you also goes out to my parents Hedwig Illerhaus and Dietmar Illerhaus for their continued support and patience during my

prolonged and bumpy studies and especially for supporting me so strongly during the time of my diploma thesis and thereby making it possible for me to focus only on my work.

And finally a very special thank you to my uncle, Prof. Dr. Gerald Illerhaus for inspiring me to work in fusion.

Bibliography

[1] H. Zohm, *Magnetohydrodynamic stability of tokamaks* (Wiley-VCH, Weinheim, 2015).

[2] J. Wesson and D. Campbell, *Tokamaks*, *Oxford Engineering Science Series* (Clarendon Press, New York, 1997).

[3] J. P. Freidberg, *Plasma Physics and Fusion Energy* (Cambridge University Press, New York, 2007).

[4] ASDEX Upgrade team, ASDEX-Upgrade drawing Gallery, 2011.

[5] P. McCarthy, IPP-Report **85/5**, (1999).

[6] K. Lackner, Computer Physics Communications **12**, 33 (1976).

[7] R. Fischer *et al.*, Fusion Science and Technology **69**, 526 (2016).

[8] R. Fischer, in *43rd EPS Conference on Plasma Physics* (European Physical Society, Geneva, Leuven, Belgium, 2010), proc. of the 43rd EPS Conference on Plasma Physics.

[9] R. Fischer *et al.*, Fusion Science and Technology **58**, 675 (2010).

[10] R. Fischer, private communication.

[11] L. Giannone *et al.*, Review of Scientific Instruments **87**, 053509 (2016).

[12] L.Giannone *et al.*, *Europhysics Conference Abstracts (CD-ROM, Proc. of the 37th EPS Conference on Plasma Physics, Dublin, Ireland, 2010)* (European Physical Society, Geneva, Ireland, 2010), No. P4, p. 122.

[13] O. Gruber *et al.*, Plasma Physics and Controlled Fusion **35**, B191 (1993).

[14] ASDEX Upgrade team, ASDEX-Upgrade drawing Gallery, 2011.

[15] M. Weiland *et al.*, Nuclear Fusion **58**, 082032 (2018).

[16] B. Kurzan and H. D. Murmann, Review of Scientific Instruments **82**, 103501 (2011).

[17] R. M. McDermott *et al.*, Review of Scientific Instruments **88**, 073508 (2017).

[18] R. J. Fonck, D. S. Darrow, and K. P. Jaehnig, Phys. Rev. A **29**, 3288 (1984).

[19] R. Fischer *et al.*, in *45th EPS Conference on Plasma Physics* (European Physical Society, Prague, 2018), proceedings of the 45th EPS Conference on Plasma Physics.

[20] R. Fischer *et al.*, in *36th European Physical Society Conference on Plasma Physics. Contributed Papers, European Physical Society (2009)* (Mateev, M.; Benova, E., Sofia, Bulgaria, 2009).

[21] S. K. Rathgeber *et al.*, Plasma Physics and Controlled Fusion **52**, 095008 (2010).

[22] F. M. Levinton *et al.*, Phys. Rev. Lett. **63**, 2060 (1989).

[23] O. P. Ford *et al.*, Review of Scientific Instruments **87**, 11E537 (2016).

[24] A. Mlynek *et al.*, First results from the new sub-millimeter polarimeter on the ASDEX Upgrade tokamak, 2016, proc. of the 21st Topical Conference on High Temperature Plasma Diagnostics (HTPD 2016).

[25] A. Bock *et al.*, Nuclear Fusion **57**, 126041 (2017).

[26] A.Kallenbach *et al.*, in *28th EPS Conference on Plasma Physics*, *Proc. of the 28th EPS Conference on Plasma Physics* (European Physical Society, Madeira, Portugal, 2001).

[27] P. C Stangeby, *The Plasma Boundary of Magnetic Fusion Devices. Series: Series in Plasma Physics, ISBN: 978-0-7503-0559-4. Taylor & Francis, Edited by Peter Stangeby, vol. 7* (Institute of Physics Publishing, Bristol, UK, 2002).

[28] A. DeSilva, Contributions to Plasma Physics **40**, 23 (2000).

[29] P. A. Schneider (unpublished).

[30] M. Hosner, private communication.

[31] D. Silvagni, private communication.

[32] T. Eich *et al.*, Nuclear Fusion **53**, 093031 (2013).